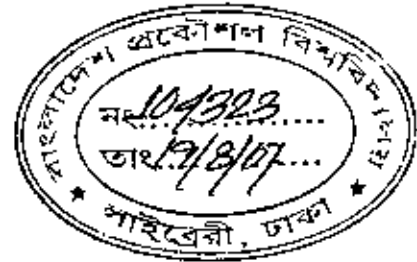


NUMERICAL STUDY OF THE COOLING CAPACITY AND PRESSURE DROP IN A HYBRID CLOSED CIRCUIT COOLING TOWER

by



MOHAMMAD RAHIS MIAH

Student no. 040309012

Registration No. 0403457, Session: April-2003

MASTER OF PHILOSOPHY
IN
MATHEMATICS



Department of Mathematics
BANGLADESH UNIVERSITY OF ENGINEERING AND
TECHNOLOGY, DHAKA-1000

July- 2007



The thesis titled

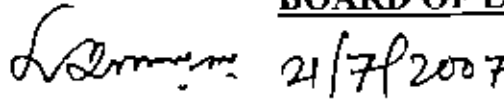
Numerical Study of the Cooling Capacity and Pressure drop in a Hybrid Closed Circuit Cooling Tower

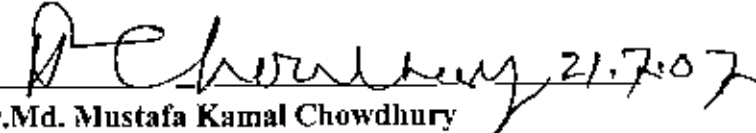
Submitted by
Mohammad Rahis Miah

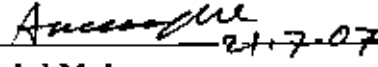
Student no. 040309012, Registration No. 0403457, Session: April-2003, a part time student of M.Phil (Mathematics) has been accepted as satisfactory in partial fulfillment for the degree of

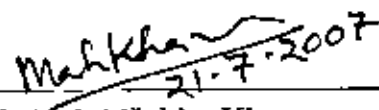
Master of Philosophy in Mathematics
21st July-2007

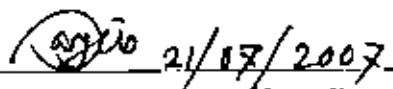
BOARD OF EXAMINERS

1.  21/7/2007

Dr. Md. Manirul Alam Sarker Chairman
Associate Professor (Supervisor)
Department of Mathematics, BUET, Dhaka-1000.
2.  21.7.07

Dr. Md. Mustafa Kamal Chowdhury Member
Professor and Head (Ex-Officio)
Department of Mathematics, BUET, Dhaka-1000.
3.  21.7.07

Dr. Md. Abdul Maleque Member
Professor
Department of Mathematics, BUET, Dhaka-1000.
4.  21.7.2007

Dr. Md. Abdul Hakim Khan Member
Professor
Department of Mathematics, BUET, Dhaka-1000.
5.  21/07/2007

Dr. Sanjib Chandra Chowdhury Member
Assistant Professor (External)
Department of Mechanical Engineering, BUET, Dhaka-1000.

Abstract

Numerical investigation on the Hybrid Closed Circuit Cooling Tower (HCCCT) having a rated capacity of 2RT has been done in this study. Here flow characteristics have been analyzed using generalized non-orthogonal coordinate system as the problem demanded. The internal flow fields have been studied by solving the laminar type viscous model and the problem related to pressure velocity coupling was handled using the Semi-Implicit Method for Pressure Linked Equations (SIMPLE) algorithm. In a HCCCT, process fluid remains completely isolated from the ambient air, so the quality of the process fluid is protected, and airborne contaminants are prevented from entering and fouling the system. HCCCT can provide clean process fluid to the system and reduces system maintenance costs and water treatment costs for evaporative equipment. Dry mode operation can conserve water and treatment chemicals, prevent icing, plume and allow variable speed pumping, thereby conserve energy. The performance characteristics of the HCCCT were numerically investigated using nominal operating condition. The heat transfer pipe used in this simulation is a bare-type copper coil having an outer diameter of 16mm. The pressure drop and cooling capacity were studied having air inlet located both at side wall and at the bottom end for different transverse pitches for various velocities. The numerical simulation demonstrated that when air is supplied from the side wall of the HCCCT, the pressure drop can be over estimated and the cooling capacity of the tower can be under estimated mainly due to non-uniform air flow distribution across the coil bank. The result obtained from this study is supposed to provide basic data which could be referred for the optimum design of the hybrid closed circuit cooling towers.

Author's Declaration

I am hereby declaring that the work in this dissertation is being carried out in accordance with the regulations of Bangladesh University of Engineering and Technology (BUET), Dhaka, Bangladesh. The work is also original except where indicated by and attached with special reference in the context and no part of it has been submitted for any attempt to get others degrees or diplomas.

All views expressed in the dissertation are those of the author and in no way or by no means represent those of Bangladesh University of Engineering and Technology, Dhaka. This dissertation has not been submitted to any other University for examination either in home or in abroad.



(Mohammad Rahis Miah)

Date: 21st July 2007

This work is dedicated to my late reverend-
Mother

Acknowledgements

It's my great pleasure to express my greatest gratitude to the Almighty for His endless blessings. I would like to have the opportunity to express my heart-rending appreciation and thoughtful sense of gratitude to my Supervisor Dr. Md. Manirul Alam Sarker, Associate Professor, Department of Mathematics, BUET who has encouraged and rightly initiated me to step into the wide arena of mathematics and its application in the engineering fields. I am immensely indebted for his expert advice and constant supervision.

I am also deeply indebted to Prof. Dr. Md. Mustafa Kamal Chowdhury, Head of the Department of Mathematics, BUET, Prof Dr. Md. Abdul Maleque and Prof. Dr.Md. Abdul Hakim Khan, Department of Mathematics, BUET, Dhaka-1000 for their liberal co-operation, encouragement and assistance of all kinds during my course of M.Phil degree.

I also would like to thank to all other teachers and other concerned with this department for their help and co-operation. Also thanks to my colleagues for their visionary encouragement to complete the M.Phil degree.

Finally, I must acknowledge my debt to my parents for whom I have been able to see the beautiful sights and sounds of the world. Last but not the least, the continuous patience, rational realization and unlimited encouragement of my wife and our only daughter Labiba Mahjabin Sheen are highly appreciated.

Contents

Abstract	iii
Author's Declaration	iv
Acknowledgements	vi
Nomenclature	ix
List of Figures	x
List of Tables	x
<hr/>	
Chapter One	1
<hr/>	
1.1 Introduction	1
1.2 Background of the study	1
1.3 A look over the numerical studies and CFD simulations	6
1.4 The concept of hybrid closed circuit cooling tower	9
1.5 Objective of the present study	13
<hr/>	
Chapter Two	14
Discretization equation for the hybrid closed circuit cooling tower	14
<hr/>	
2.1 Introduction	14
2.1.1 Basic equations in generalized coordinates	14
2.1.2 Numerical treatment: Nomenclature of the cell	16
2.1.3 Need for the transformation	17
2.1.4 Area of the cell	20
2.2 Discretization equations	21
2.3 Discretization equation for u	23
2.4 Discretization equation for v	28

2.5 Discretization of the energy equation	29
2.6 Relaxation and convergence criteria	33
2.7 The pressure equation; Pressure based algorithm-SIMPLE	33
2.8 Code validation	33
2.9 Conclusion	36
<hr/>	
Chapter Three	37
Numerical simulation of the hybrid closed circuit cooling tower	37
<hr/>	
3.1 Introduction	37
3.2 Numerical analysis of the cooling tower in dry mode	37
3.2.1 Simulation of the HCCCT having a rated capacity of 2 RT	37
3.2.2 The flow characteristics inside HCCCT with a capacity of 2 RT	38
3.2.3 Temperature distribution in 2 RT tower w.r.t. air inlet velocity	39
3.2.4 Temperature drop w.r.t. cooling water inlet temperature	40
3.2.5 Temperature drop w.r.t. air inlet temperature	41
3.2.6 Pressure drop due to different arrangement of coil pitch having the air inlet at the side wall.	42
3.3 Numerical study of the wet closed cooling tower	43
3.4 Conclusion	48
<hr/>	
Chapter Four	49
Conclusion	49
<hr/>	
4.1 Summary of the thesis	49
<hr/>	
4.2 Future work	50
<hr/>	
References	51
<hr/>	

NOMENCLATURE

A	: Effective cross section area of cooling tower [m^2]
a	: Effective interfacial area per unit volume [m^2/m^3]
c_p	: Specific heat at constant pressure [kJ/kgK]
d	: Tube diameter [m]
G	: Flow rate of air [kg/h]
k	: Turbulence kinematic energy [m^2/s^2]
Q	: Cooling capacity [kcal/h]
T	: Temperature [K]
v	: Volume of heat exchanger [m^3]
w	: Flow rate of cooling water [kg/h]

Greek Symbols

μ	: The viscosity of the fluid [kg/(m.s)]
ν	: Kinematic viscosity [m^2/s]
ρ	: The density of the fluid [kg/ m^3]

Dimensionless numbers

Pr	: Prandtl number
Re	: Reynolds number

List of Figures

Fig. 1.1 A conceptual HCCCT	10
Fig. 1.2 A schematic model of HCCCT	11
Fig. 2.1 A typical cell view with surfaces	17
Fig. 2.2 Cell and surface numbering	17
Fig. 2.3 Grid representation (a) physical plane, (b) computational plane	18
Fig. 2.4 Unit normal vectors on the corresponding surfaces	19
Fig. 2.5 Surface vectors in terms of components	20
Fig. 2.6 Area of a typical cell	20
Fig. 2.7 An internal control volume with interior grid point P along with four neighbors	26
Fig. 2.8 Flowchart of the program based on generalized non-orthogonal coordinate.	32
Fig. 2.9 A lid driven square cavity along with boundary conditions	34
Fig. 2.10 Comparative u-velocity at vertical centerline of the cavity	35
Fig. 3.1 Schematic of the HCCCT	38
Fig. 3.2 Velocity vector inside 2 RT HCCCT	39
Fig. 3.3 Temperature distribution w.r.t. air inlet velocity	40
Fig. 3.4 Temperature drop w.r.t cooling water inlet temperature	40
Fig. 3.5 Temperature distribution w.r.t. air inlet temperature	41
Fig. 3.6 Pressure distribution w.r.t. the coil pitch	42
Fig. 3.7 The temperature range of the cooling water w.r.t. WBT	46
Fig. 3.8 The cooling capacity in wet mode operation w.r.t. WBT	47
Fig. 3.9 Pressure drop inside 2RT HCCCT in wet mode	47

List of Tables

Table 3.1 Geometric parameters of the 2 RT HCCT	37
Table 3.2 Simulation condition for the 2 RT HCCCT	38



1.1 Introduction

The twentieth century saw tremendous advances in technology and economic well being around the world. Now as we entered a new century and a new millennium, it holds the promise of even greater achievements and challenges. For our economic well being to continue, we need to pay close attention to the effect of technology on the environment and to the wise use of energy resources. We are turning our attention to recycling, sustainable development, and use of renewable energy and to increase energy efficiency. Recent decades have seen the introduction and rapid growths in the use of cooling towers to reject heat, cool buildings and reduce the temperature of water circulated through various heat rejection equipments. Energy efficiency, environmental benefits and effectiveness in heating and cooling are among the reasons for the popularity of these systems with consumers.

1.2 Background of the study

Cooling tower is a relatively inexpensive and dependable heat rejection device. It renders down waste heat to the atmosphere through the cooling of a water stream to a lower temperature. Evaporative heat rejection equipments like cooling towers are commonly used to provide significantly lower water temperatures than achievable with air cooled or dry heat rejection devices, like the radiator in a car, thereby achieving more cost-effective and energy efficient operation of systems in need of cooling. The cooling potential of a wet surface is much better than a dry one. Cooling towers are commonly used for providing cooled water for air-conditioning, manufacturing and electric power generation. The smallest cooling towers are designed to handle water streams of only a few gallons of water per minutes supplied in small pipes like those might see in a residence, while the largest cooling towers cool hundreds of thousands of gallons per minutes supplied on a large power plant through pipes having a diameter of as much as 5 meters.

A remedy from thermal pollution

Warm water can be found in a number of different areas in nature such as hot springs or water warmed by volcanic activity and when it is produced by human while using water

for cooling power plants or other industrial applications is discharged into streams, rivers, and lakes and is regarded as a problem. This is known as thermal pollution or thermal discharge and it is introduction of waste heat into bodies of water that support aquatic life. In addition, warmer water allows bacterial populations to increase and thrive and algae "blooms" may occur. In developed countries like USA, regulators and lawmakers recognized that thermal pollution is a problem and addressed the issue on EPA (Environment Protection Agency) as Clean Water Act. States and other regulatory agencies use those guidelines to require power plants and industries to limit warm water discharges back into surface waters, sometimes by way of cooling towers.

Growing need for towers especially for power plants

According to the U.S Geological Survey, about 48% of all freshwater and saline-water withdrawals for 2000 were used for thermoelectric power. Most of this water was derived from surface water and used for once through cooling at power plants. About 52% of fresh surface-water withdrawals and about 96% of saline-water withdrawals were for thermo-electric power use. This large amount of water is needed by power plants due to the fact that over the years, there has been an ever-increasing need for electricity. This means power plants are expected to run at near maximum output for a large part of the year. The cheapest and easiest method for power plants to operate has always been to withdraw water from a nearby body of water, pass it through the plant and then reject the heated water to the same body of water. These once-through cooling systems now require very strict environmental permits; some permits require that the plant must discharge the water within a temperature differential limit over the temperature of the intake water. Cooling towers provide a way in which power plants can follow permit restrictions. Cooling towers can greatly solve thermal pollution problems because the cooling results can be predicted with a high degree of accuracy even prior to installing the towers.

Cooling towers are used frequently because they allow the user to reject heat from a system or process without consuming excessive quantities of water or thermally polluting a body of surface water. There are minor drawbacks, which are usually accepted as the price of the larger benefit.

These drawbacks are:

- Higher operating temperatures than would be obtained from surface water or municipal water; resulting in some loss of thermodynamic efficiency;
- Cost of electricity to run fans;
- Drift, the discharge of minute water droplets which contain minerals and other impurities;
- Cost of water treatment to prevent corrosion, scale, and biological fouling of equipment; and
- Risk of dispersion of airborne pathogens from poorly maintained cooling towers.

Cooling towers: The basics and purposes

All most all air-conditioning & refrigeration systems and industrial processes generate heat that must be removed and dissipated. In general, air-conditioning and refrigeration systems in excess of 150-200 ton (528-704kW) capacities make use of water as the medium for heat rejection and the majority of such installations utilize cooling towers for the ultimate rejection of this heat to the atmosphere. In smaller systems, air-cooled heat exchanger and evaporative condensers are increasing in use but cooling towers continue to be the method of choice where limiting the energy usage is a primary consideration.

In the most part of the past century, removing heat from refrigerant condensers or industrial process heat exchangers was accomplished by drawing a continuous stream of a water from a utility water supply or a natural body of water, heating it as it passed through the process and then discharging the water directly to the body of water. Water purchased from utilities has become prohibitively expensive because of increased cost for water supply as well as disposal. Similarly, cooling water drawn from natural sources is relatively unavailable because the disturbance to the ecology of the water source caused by the increased temperature of discharged water has become unacceptable.

Cooling towers are commonly used as a medium to dissipate heat from water-cooled refrigeration, air-conditioning and industrial process systems. The water consumption rate of a cooling tower system is only about 5% of that of a once-through system, making it the least expensive system to operate with purchased water supplies. In addition, the amount of heated water discharged (blow-down) is very small, so the ecological effects like GWP

(Global Warming Potential) and ODP (Ozone Depletion Potential) are greatly reduced. Cooling tower can be defined as a device whose main purpose is to cool water circulated through condensers or other heat-rejection equipment, by direct contact between the water and a stream of air.

A cooling tower cools water by a combination of heat and mass transfer. The water to be cooled is distributed in the tower by spray nozzles, splash bars, or film-type fill, which exposes a very large water surface to atmospheric air. Atmospheric air is circulated by (1) fans, (2) convective currents, (3) natural wind currents or (4) induction effect from sprays. A portion of the water absorbs heat to change heat from a liquid to a vapor at constant pressure. This heat of vaporization at atmospheric pressure is transferred from the water remaining in the liquid state into the air stream.

Cooling tower related widely used terms

The generic term cooling tower is used to describe both direct (open circuit) and indirect (closed circuit) heat rejection equipment. Before giving a rigorous classification of the towers, some useful terms those will be repeatedly used in this study are going to be discussed next.

Drift: Drifts are water droplets that are carried out of the cooling tower with the exhaust air. Drift droplets have the same concentration of impurities as the water entering the tower. The drift rate is typically reduced by employing baffle-like devices, called drift eliminators, through which the air must travel after leaving the fill and spray zones of the tower.

Blow-out: By blow-out we mean water droplets those are blown out of the cooling tower by wind, generally at the air inlet openings. In the absence of wind, water may also be lost through splashing or misting. Devices such as windcreens, louvers, splash deflectors and water diverters and applied to reduce these losses.

Plume: Plume means the stream of saturated exhaust air leaving the cooling tower. The plume is visible when water vapor it contains condenses in contact with cooler ambient air, like the saturated air in one's breath fogs on a cold day. Under certain conditions, a cooling tower plume may represent fogging or icing hazards to its surroundings. It can be mentioned here that the water evaporative in the cooling process is "pure" water, in contrast to the very small percentage of drifts droplets or water blown out of the air inlets.

Blow-down: By blow-down we mean the portion of the circulating water flow that is removed in order to maintain that the amount of dissolved solids and other impurities at an acceptable level.

Noise: Noise is the sound energy emitted by a cooling tower and heard (recorded) at a given distance and direction. The sound is generated by the impact of falling water, by the movement of air by fans, the fan blades moving in the structure, and the motors, gearboxes or drive belts.

Types of cooling towers

There are two types of cooling towers, namely, direct contact or open cooling tower that exposes the water directly to the atmosphere and transfers source heat load directly to the air. The other type called closed circuit cooling tower (CCCT), which maintains an indirect contact between the fluid and the atmosphere. Cooling towers can be categorized from various perspectives like depending on air circulation, air and water flow direction, heat transfer mode etc. Depending on air circulation/draft, towers are known as Atmospheric type or Non-Mechanical Draft towers and, Mechanical draft towers. Atmospheric or natural draft towers utilize natural convection, so it is devoid of any fill and don't use any mechanical device for air movement. Depending on the air and water flow, towers are called crossflow type where air flows in horizontal direction across the downward falling water and counterflow type where air flows vertically upward through the fill, counter to the falling water. Depending on heat transferring mode, cooling towers are respectively called wet tower when evaporative cooling is used, dry tower when air blast cooling is utilized and wet-dry type which has the simultaneous characteristics of both dry and wet towers. Cooling effects in wet cooling towers are partially brought about by the evaporative condenser where a quota of the circulating water gets evaporated and partially by the sensible heat transfer. On the other hand, cooling effect is attained through convection and radiation heat transfer from any hot metal surface to an air stream moving across the surface and finally dissipating the heat into the atmosphere.

Review of the previous studies

The cooling tower related research works can be broadly divided into two categories namely, the experimental studies and the numerical simulations.

1.3 A look over the numerical studies and CFD simulations

Bergstrom et al. [1] presented a finite volume prediction for wind flow over an induced draft counter flow-cooling tower where they implemented the cooling tower structure as a series of internal boundaries for which the discrete transport equations are modified to yield the appropriate boundary conditions for the velocity and pressure. Their numerical prediction indicated that the wind significantly increases the flow rate through the windward intake. Bender et al. [2] made predictions with the protective wind wall and claimed that the computational code shows the wind to have a significant effect on the cooling tower intakes. Bornoff et al. [3] presented the results of a numerical investigation into the interaction of two adjacent plumes in a cross-flow. The computations are performed for three-dimensional, turbulent, buoyant and interacting plumes. They used a low Reynolds number k- ϵ turbulence model with hybrid and QUICK discretization schemes.

Majumdar et al. [4] presented an advanced pressure model, which computes the two-dimensional distributions of air velocity, temperature, pressure, and moisture content; and water temperature. Their model is embodied into a computer code, which is applicable for the natural, and mechanical draft towers for both the crossflow and counterflow arrangements.

Hawladar and Liu [5] reported the mathematical and physical models governing the flow, mass and heat energy of moist for an evaporative natural draft-cooling tower. The models consider the effect of non-spherical shape of water drops on the flow; heat and mass transfer and they claimed that the difference between the measured and the predicted outlet water temperature is 0.26°C. Their simulation proves that the main transfer processes take place in the fill region where the percentage of latent heat transfer is predicted as 83%. They predicted the hourly performance of a natural draft-cooling tower under the meteorological condition of Singapore.

Dreyer and Erens [6] developed a mathematical model and a computer simulation program for the modeling of counterflow cooling tower splash pack thermal performance and

reported that the model predicts the correct trends for both the transfer characteristics and the pressure drop across the packing material.

Rehman et al. [7] reported a model of counter flow wet cooling towers where they verified the authenticity of the model comparing the values of number of transfer units (NTU) and tower effectiveness (ϵ) with the commonly described models. They reported an appreciable difference in NTU and ϵ values if the resistance to heat transfer in the water film and non-unity of Lewis is number is considered.

Hasan and Guohui [8] presented the theoretical analysis and computational modeling of closed wet cooling towers. They also showed that the maximum difference in the calculated cooling water heat or air sensible heat between the two proposed simplified methods and a general computational model less than 3% and that CFD results agreed well with the analytical results when the air is supplied from the bottom of the tower.

Jaber and Webb [9] incorporated the effectiveness (ϵ) and NTU's definition for heat exchanger design with those to the cooling tower operating conditions. They ignored the heat transfer resistance in the air- water interface and the effect of water evaporative on the air process states and used Merkel's approximation of replacing the sum of the single-phase heat transfer from the water-air interface to the air. Optimum utilization of the CFD for prediction the thermal performance of closed wet cooling towers has been reported by number authors including Gan et al. [10].

Eldessouky et al. [11] reported a theoretical investigation for the steady-state counter flow wet cooling tower with modified definition for NTU and effectiveness. They developed a new relation among the tower effectiveness and the modified NTU and the capacity rate ratio. They also outlined a procedure for implementing the model in designing or rating cooling towers.

Soylemez [12] developed formulae for forced draft counter-current cooling towers for the best thermo economical performance as a design point and presented a thermo-hydraulic performance point of counter current mechanical draft wet cooling towers using effectiveness-NTU method along with the derivation of psychrometric properties of moist air based on numerical approximation method.

Kloppers and Krogger [13] reported a detained derivation of the heat and mass transfer equations of evaporative cooling in wet-cooling towers. The differences in the heat and mass

transfer analyses and solution techniques of the Merkel and Poppe methods are described in terms of enthalpy diagrams and psychrometric charts and they extended the psychrometric chart to accommodate air in the supersaturated state.

Kaiscr et al. [14] developed a numerical model for studying the evaporative cooling processes that take place in a hydrosolar roof type cooling tower which present lower droplet fall and uses renewable energy instead of fans to generate the air mass flow within the tower. The numerical results showed the strong influence of the average water drop size on efficiency of the system and reveal the effect of other variables including temperature gap between water inlet temperature wet bulb temperature.

Kunxiong and Shiming [15] presented a method for evaluating the heat and mass transfer characteristics in a counter-flow reversibly used water cooling tower and reported that the method developed could be used to evaluate the thermal performance with an acceptable accuracy.

Ibrahim et al. [16] presented a model for a falling film type-cooling tower to investigate the effect of tower parameters and the effect of liquid side thermal resistance on the tower performance. They used energy equation to determine the temperature distribution across the liquid film and the heat and mass transfer processes between the liquid film and air bulk are described using three ordinary differential equations. They showed that an increase in tower characteristics KaV/L under the same conditions improves the tower performance.

Baker et al. [17] examined the effect of some of the approximations and suggested the means of minimizing the errors in predicting cooling tower performance. They also gave detail-deriving steps of Merkel's equation.

Webb and R.L. [18] performed a unified theoretical treatment for the thermal analysis of cooling towers, evaporative condensers and evaporative fluid coolers outlining the specific calculation procedures for sizing and rating each type of evaporative exchanger.

Webb and Villacres [19] reported computer algorithms for performing rating calculations of three evaporatively cooled heat exchangers. The algorithms are particularly useful for rating commercially available heat exchangers at off-design conditions. The heat and mass transfer characteristics of a particular heat exchanger is derived from the manufacture's rating data at the design point.

Al-Nimr [20] proposed a simple mathematical model to describe the dynamic thermal behavior of a counter-flow cooling tower taking into account both the sensible and latent heat cooling effects on the tower performance. He applied simple perturbation technique to solve the governing equations.

Makinejad [21] developed a new method to describe an acceptable mathematical solution for cooling towers, taking into account the main influencing parameters, the liquid to gas ratio (L/G) and the actual liquid and gas interface. He showed that the exit gas temperature is strongly influenced by the liquid inlet temperature. In case of closed loop and counter current systems, this liquid inlet temperature is more or less close to the adiabatic saturation temperature of the incoming gases.

Pascal and Dominique [22] presented a simplified model for indirect cooling towers behavior fulfilling several criteria such as simplicity of parameterization, accuracy, possibility to model the equipment under various operation conditions and short computation time. The model introduces only two parameters, air-side and water-side heat-transfer coefficients and allows one to estimate energy and water consumptions under different operating conditions such as variable wet-bulb temperatures or variable airflow rates.

1.4 The concept of hybrid closed circuit cooling tower

The concept of the closed circuit cooling tower, which combines the function of a cooling tower and heat exchanger onto one piece of equipment, was developed initially in the early 1930's and the work has continued, although somewhat sporadically, to this date. Such heat exchangers are basically wetted tube bundles whose design depend on the type of application, that is, the cooling of water, fluids other than water, or condensing refrigerant or other vapors. The closed circuit cooling towers used to cool fluids are known variously as wet surface air coolers, closed circuit coolers or industrial process coolers, while those used to condense vapors known as evaporative condensers or wet surface vapor condensers. In all cases, the fluid in the tubes never comes in contact with the atmosphere and, therefore, there is no possibility of contamination of the fluid with airborne dirt and impurities or, on the other hand, contamination of the air by the fluid.

The hybrid closed circuit cooling tower (HCCCT) is a CCGT, which is capable of working both in wet mode and in dry mode. As the word hybrid indicates, this cooling or condensing system for fluids operates as a dry cooler in winter and as an evaporative cooler

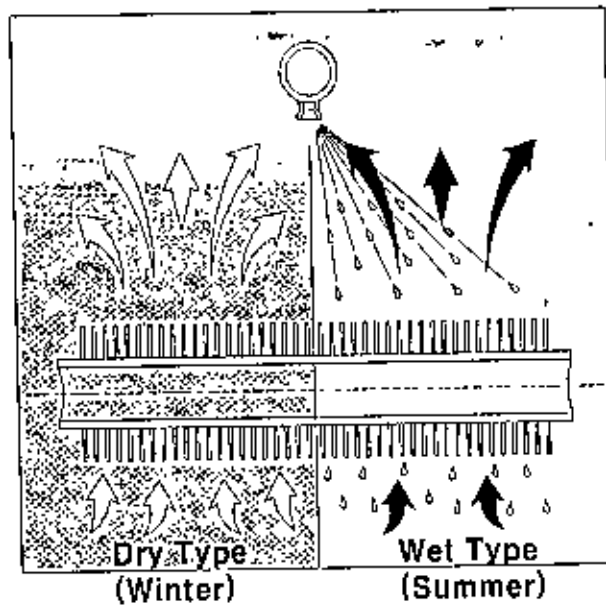


Fig. 1.1 A conceptual HCCCT

in summer by spraying on the heat transfer surface. Pumps are integrated in the product to transport water from the lower collection basin to the upper distribution basins or sprays. The internal coils can be fabricated from any of several materials, but galvanized steel copper predominate. HCCCT require a bundle closed-circuit heat exchanger (usually tubular serpentine coil bundles) that is exposed to air/water cascades similar to the filler of a cooling tower. Some types include supplemental film or splash fill sections to augment the external heat exchange surface area. There are drawbacks associated with closed-loop systems as well. Recirculating wet-cooling towers have an energy penalty associated with the additional pumps, fans, and auxiliary equipment and can also require more extensive water treatment. A conceptual hybrid closed circuit cooling tower is shown in Fig. 1.1 and a complete model has been shown in Fig. 1.2. In a HCCCT, process fluid remains completely isolated from the atmosphere, so the quality of the process fluid is protected, and air borne contaminants are prevented from entering and fouling the system and thereby reduce system maintenance, provide operational flexibility.

HCCCT can help in protecting legionella disease. Legionella is a bacterial disease which may cause pneumonia, and whose reproduction is especially favored in warm water of temperatures between 20°C and 45°C. The growth of legionella is promoted by inadequate water flow, such as in water stagnation in pipes that are only seldom used. Legionella

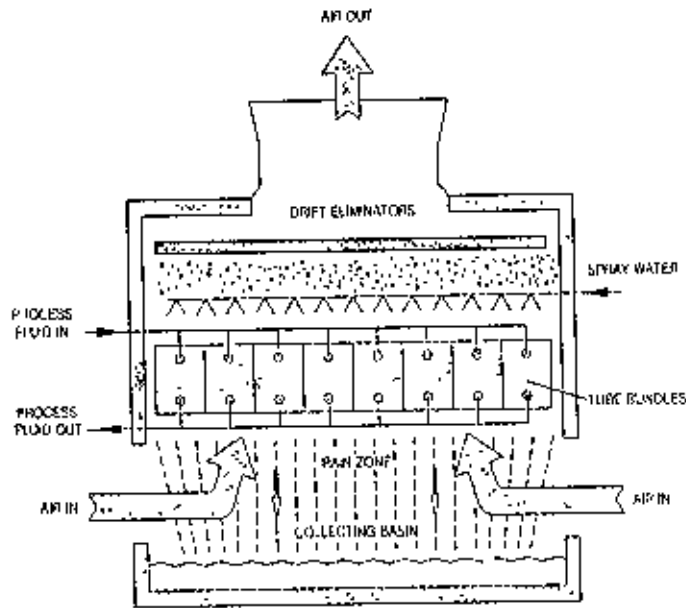


Fig. 1.2 A schematic model of HCCCT

bacteria are widely distributed in the environment, especially in hot and cold water systems, water in air conditioning cooling towers. The disease is spread through the air from a water source. Breathing in aerosols from contaminated water systems are the most likely route of transmission of infection. Since the process fluid remains confined at HCCCT, so legionella bacteria can't be spread to the environment. HCCCT can provide clean process fluid to the system and thus could extend the life of other components like condenser bundles, compressors, etc in the system and the need to shut down the system periodically to clean the heat exchanger could be dramatically reduced. HCCCT reduces system maintenance costs and water treatment costs for evaporative equipment. The dry mode operation can conserve water, prevent icing and plume and allows for variable speed pumping and thereby conserving energy.

HCCCT can be used at a number of chemical and process industries. In dyeing industries, most of the chemicals and their alloys are very sensible to temperature and humidity, HCCCT can be applied to supply the cooling effect through precisely maintaining the humidity and the temperature at the desired level. In cooling buildings especially the computer centers and other laboratories where heat is generated almost regularly, HCCCT can be very useful due to the fact that, during the summer when the cooling requirements are

higher, HCCCT can be operated in wet mode using the spray water to supply the maximum cooling effect. On the other hand, in winter, the cooling requirements are lower; therefore, HCCCT can be operated in dry mode maintaining a lower operating cost. As a source of clean cooling effect, HCCCT can be used at the hospitals keeping the sound level at a tolerable limit. The importance and the purpose for the developing of HCCCT can be made even more evident if we closely look at the critical operating conditions and requirements for the smooth functioning of HCCCT in winter and summer separately as explained next.

The typical working conditions of dry mode in winter:

- HCCCT would work well in dry mode during the mid-season and winter as soon as ambient temperature remain below 12°C
- In dry mode, no spray water, so no freezing ensures the smooth functioning of the HCCCT.
- There is no plume in winter operation.
- The power consumption by HCCCT is lower.
- Uncomfortable noise level is lower than most dry cooler.

The typical working conditions of wet mode in summer:

- HCCCT would operate smoothly in wet mode during the summer while the ambient temperature is above 12°C
- The water consumption by HCCCT is lower in wet mode.
- There is possibility to cool the process water down to 4°C above the wet bulb temperature.
- It can be packed in light and compact bundle design with optimized circuitry.

In the HCCCT, water will be sprayed in summer using squared form and wide angle spray nozzles from the top of the tower along with a counter-type of air flow in both summer and winter from the bottom part. In general, weather is warmer in summer, so both spray water and countertype air flow will be utilized to get the expected cooling effect. During the summer operation, no plume formation is expected due to the higher ambient temperature and higher dew-point temperature. In winter, only the cooled air from the bottom will be

used to get the cooling effect and plume free state is predicted once more because the local winter ambient air contain lower moisture.

1.5 Objective of the study

In few highly developed countries, the cooling tower technology is getting more and more importance day by day due to the ecology related concerns like green house effect, ODP/GWP effects. In USA, cooling tower is being used in many of the power and chemical plants for effectively rejecting heat. In East Asia, the technology and the research related to cooling tower is sparse in the relevant literature and that of HCCCT is really missing in greater scale. The objective of this research is to develop the cooling tower technology. The cooling towers are in use to this date can operate without forming plume during the mid-season and winter when ambient temperature is below 12°C. Our objective is to present the design information related to HCCCT, which would have the ability to operate in plume free mode until 15°C in dry mode. Proposed HCCCT would have a rated capacity of 2 RT.

To accomplish them, the following specific tasks have been set out:

- Derivation of the basic equations in control volume method using generalized non-orthogonal coordinate system and the hybrid scheme embodied in SIMPLE (Semi-Implicit Method for Pressure Linked Equation) algorithm of Patankar [23].
- Investigation of pressure drop from different perspectives like considering the coil's transverse pitch, variable air velocities etc. Reporting the effect of both the nozzle number and the air supply from the bottom and from the sidewall on cooling capacity and pressure drop.
- Numerical simulation of the cooling capacity and the pressure drop for the HCCCT having a rated capacity of 2RT.
- Investigation of the performance and to make sure that the HCCCT works well in plume free mode when the temperature is lower than or equal to 15°C in dry mode.

The detailed computational procedures and the results of the above mentioned tasks are discussed in the subsequent chapters.

Chapter Two

Discretization equation for the hybrid closed circuit cooling tower

2.1 Introduction

Numerical models are used to solve problems in a wide variety of areas including science and engineering. Many of these models consist of ordinary algebraic equations, differential equations, systems of equations and so on and the methods for solving such equations that can be implemented in a computer program are known as numerical methods. The analysis and application of such numerical methods are the prime focus in this chapter. To analyze the flow characteristics and the heat transfer inside the hybrid closed circuit cooling tower (HCCCT), it is imperative to derive the basic equations in generalized non-orthogonal coordinate. The first aspect is being discussed next.

2.1.1 Basic equations in generalized coordinate

The governing equations of the fluid mechanics are described here suppressing the complete derivation. The equations are presented in the descending order of complexity and the classical forms of the equations are given first and other forms specially formulated for the computational purposes follow later on. Two main problems arise while applying computational methods to practical flow situations, first one is the geometrical complexity of the domains in which the most practical flow occurs and the second one is the degree of physical complexity of the flow. The first aspect is the main focus of this section and the second one will be handled next.

Since the dimension along the HCCCT, length is large compared to the width, steady and stabilized sprayed water flow from the squared form and wide-angled spray nozzles can be considered to have the 2-dimensional flow without the loss of generality. To capture the geometrical complexity of the HCCCT, we have to solve the 2-dimensional Navier-Stokes (N-S) equations using the body-fitted coordinate system. The control Volume Method was used for discretizing the partial differential equations and SIMPLE (Semi-Implicit Method for Pressure Linked Equations) algorithm of Patankar [23] was followed to overcome the difficulties related to pressure-velocity coupling. A bit of details of the procedures are given in subsequent sections.

General form of a conservation law in two-dimensional contexts

The basic equations of fluid dynamics are based on the three following universal laws of conservation:

- Conservation of Mass
- Conservation of Momentum
- Conservation of Energy

Compact form of the conservation equations:

It is required to combine all the basic equations and to put in a compact vector form to facilitate the computation with the help of some numerical algorithm. Using vector notation, the compressible Navier-Stokes (N-S) equations in Cartesian coordinates can be written as

$$\frac{\partial Q}{\partial t} + \frac{\partial E}{\partial x} + \frac{\partial F}{\partial y} = \frac{\partial E_v}{\partial x} + \frac{\partial F_v}{\partial y} + S \quad (2.1.1)$$

where $Q = [\rho \ \rho u \ \rho v]^t$ and the inviscid-flux vector terms E, F are given by

$$E = \begin{bmatrix} \rho u \\ \rho u^2 + P \\ \rho uv \end{bmatrix}, \quad F = \begin{bmatrix} \rho v \\ \rho vu \\ \rho v^2 + P \end{bmatrix} \quad (2.1.2)$$

Here, the first row of the vector equation corresponds to the continuity equation and second and third rows are the momentum equations. It is often easier to code the desired numerical algorithm when N-S equation is written in this compact vector-matrix notation. The viscous-flux vectors E_v and F_v are expressed as

$$E_v = \begin{bmatrix} 0 \\ \tau_{xx} \\ \tau_{xy} \end{bmatrix}, \quad F_v = \begin{bmatrix} 0 \\ \tau_{yx} \\ \tau_{yy} \end{bmatrix} \quad (2.1.3)$$

The symmetric stress tensors τ_{ij} are written as follows

$$\begin{aligned} \tau_{xx} &= \frac{4}{3}\mu \frac{\partial u}{\partial x} - \frac{2}{3}\mu \frac{\partial v}{\partial y} \\ \tau_{yy} &= \frac{4}{3}\mu \frac{\partial v}{\partial y} - \frac{2}{3}\mu \frac{\partial u}{\partial x} \\ \tau_{xy} &= \tau_{yx} = \mu \left(\frac{\partial v}{\partial x} + \frac{\partial u}{\partial y} \right) \end{aligned} \quad (2.1.4)$$

τ_{xx} , τ_{yy} can also be written alternatively as

$$\begin{aligned}\tau_{xx} &= 2\mu \frac{\partial u}{\partial x} - \frac{2}{3}\mu \frac{\partial u}{\partial x} - \frac{2}{3}\mu \frac{\partial v}{\partial y} \\ &= 2\mu \frac{\partial u}{\partial x} - \frac{2}{3}\mu \left(\frac{\partial u}{\partial x} + \frac{\partial v}{\partial y} \right) \\ &= 2\mu \frac{\partial u}{\partial x} - \frac{2}{3}\mu \nabla \cdot \bar{U}\end{aligned}\quad (2.1.5)$$

$$\begin{aligned}\tau_{yy} &= 2\mu \frac{\partial v}{\partial y} - \frac{2}{3}\mu \frac{\partial u}{\partial x} - \frac{2}{3}\mu \frac{\partial v}{\partial y} \\ &= 2\mu \frac{\partial v}{\partial y} - \frac{2}{3}\mu \left(\frac{\partial u}{\partial x} + \frac{\partial v}{\partial y} \right) \\ &= 2\mu \frac{\partial v}{\partial y} - \frac{2}{3}\mu \nabla \cdot \bar{U}\end{aligned}\quad (2.1.6)$$

where $\bar{U} = u\hat{i} + v\hat{j}$. Equation (2.1.1) without any source term can be rewritten in compact form as

$$\frac{\partial Q}{\partial t} + \frac{\partial}{\partial x}(E - E_v) + \frac{\partial}{\partial y}(F - F_v) = 0 \quad (2.1.7)$$

$$\Rightarrow \frac{\partial Q}{\partial t} + \nabla \cdot \bar{W} = 0 \quad (2.1.8)$$

where $\bar{W} = (E - E_v)\hat{i} + (F - F_v)\hat{j}$. Integrating eqn. (2.1.8), we have

$$\int_V \frac{\partial Q}{\partial t} dv + \int_V \nabla \cdot \bar{W} dv = 0 \quad (2.1.9)$$

With the help of Gauss Divergence theorem, we finally get

$$\int_V \frac{\partial Q}{\partial t} dv + \int_S \bar{W} \cdot \bar{n} ds = 0 \quad (2.1.10)$$

where \bar{n} is the normal vector in the outward direction to the surface dS ; S is the whole surface that bounds the control volume (CV).

2.1.2 Numerical treatment: Nomenclature of the cell

The cell and the surface orientation is given next. A control volume is referred to as cell and bounding line or curves are being called surfaces. Line or curve would have been more

appropriate in place of surface for two-dimensional cases, yet the word surface has been used to facilitate the extension of the concept to the three-dimensional case where we should have six 2-dimensional surfaces. It may be noted that in a two-dimensional cell, there are four surfaces of unit width. A typical cell and along with its surfaces are shown in Fig 2.1.

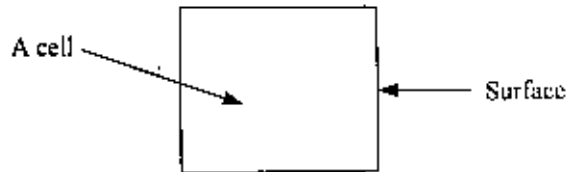


Fig. 2.1 A typical cell view along with surfaces

Numbering system of the cell

In Fig 2.2, the numbering system of cell and the surfaces are shown. Here n is located at right upper corner of a typical cell or surface. Therefore, $n-ii$ is located just left of n and $n+ii$ is positioned at right of n in ξ -direction.

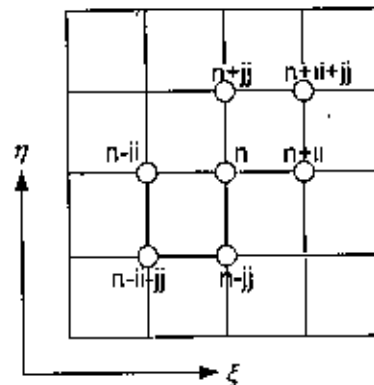


Fig. 2.2 Cell and surface numbering

Similar arguments apply for the components in η -direction.

2.1.3 Need for the transformation

So far, the basic equations of fluid mechanics have been expressed in terms of a Cartesian coordinate system and typically the computational domain is considered to be rectangular in shape. Unfortunately, most of the physical domains of interest are non-rectangular.

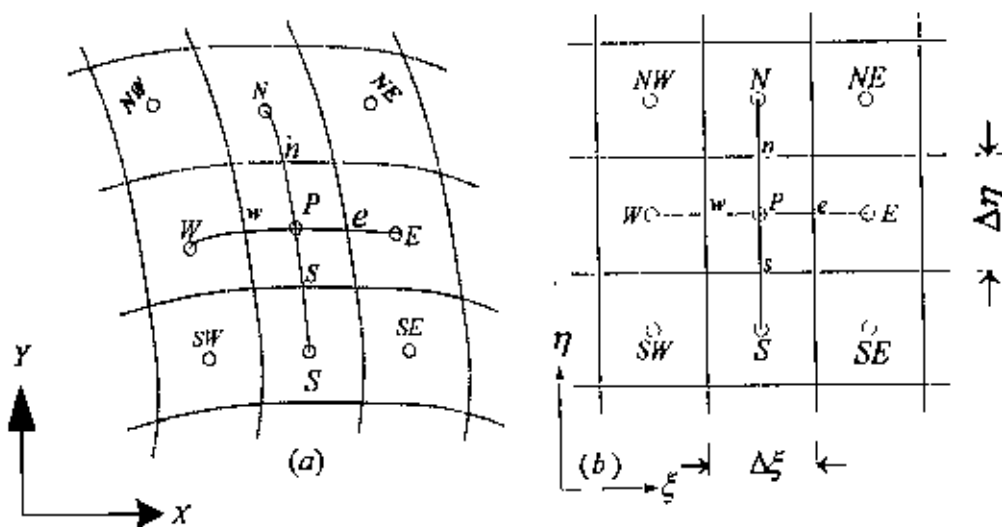


Fig.2.3 Grid representation (a) physical plane, (b) computational plane

Imposing a rectangular computational domain on such a physical domain needs some sort of interpolation in order to implement the boundary condition. Boundary conditions have important influence on the solution of the equations and inaccuracies especially in case of the higher sensitivity could arise due to such interpolation. Moreover, unequal grid spacing near the boundaries creates further complications. To overcome these difficulties, mapping or transforming the physical domain to a computational domain is required. This is accomplished by specifying a generalized coordinate system that maps the nonrectangular grid system from the physical space to the rectangular grid spacing in the computational space. A typical physical and a computational domain are shown in Fig. 2.3 where a computational domain is derived by deforming the physical domain. It may be noted here that the form and the type of the transformed equation remains the same as that of the original equation. The numerical generation of curvilinear coordinate systems is widely considered as one of the primary pacing items in CFD.

A body-fitted coordinate system is a curvilinear coordinate system having some coordinate line coincident with each segment of the boundary of a region. Let us introduce the general transformation, to define the relations between the physical and the computational spaces, as follows:

$$\begin{aligned} \xi &= \xi(x, y) \\ \eta &= \eta(x, y) \end{aligned}$$

Then for a two dimensional cell, we should have

$$\int_V \frac{\partial Q}{\partial t} dv + \int_{S_\xi} \vec{W} \cdot \vec{n}_\xi ds_\xi + \int_{S_\eta} \vec{W} \cdot \vec{n}_\eta ds_\eta = 0 \quad (2.1.11)$$

where the terms having subscripts ξ and η represent quantities along the stream wise and cross-stream wise directions respectively. The outward-drawn unit normal vectors as shown in Fig. 2.4 & Fig. 2.5 can be written as

$$\begin{aligned} \vec{n}_\xi &= (S_\xi \hat{i} + S_\xi \hat{j}) / |\vec{S}_\xi| \\ \vec{n}_\eta &= (S_\eta \hat{i} + S_\eta \hat{j}) / |\vec{S}_\eta| \end{aligned} \quad (2.1.12)$$

The surface vectors \vec{S}_ξ , \vec{S}_η as shown in Fig. 2.5 can be given by

$$\begin{aligned} \vec{S}_\xi &= \begin{vmatrix} \hat{i} & \hat{j} \\ x_3 - x_4 & y_3 - y_4 \end{vmatrix} \\ &= (y_3 - y_4) \hat{i} - (x_3 - x_4) \hat{j} = S_{\xi_x} \hat{i} + S_{\xi_y} \hat{j} \end{aligned}$$

In a similar fashion

$$\begin{aligned} \vec{S}_\eta &= \begin{vmatrix} \hat{i} & \hat{j} \\ x_2 - x_3 & y_2 - y_3 \end{vmatrix} \\ &= (y_2 - y_3) \hat{i} - (x_2 - x_3) \hat{j} = S_{\eta_x} \hat{i} + S_{\eta_y} \hat{j} \end{aligned}$$

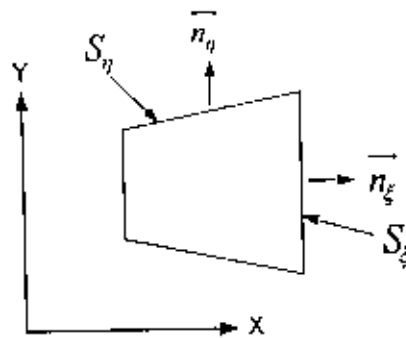


Fig. 2.4 Unit normal vectors on the corresponding surfaces

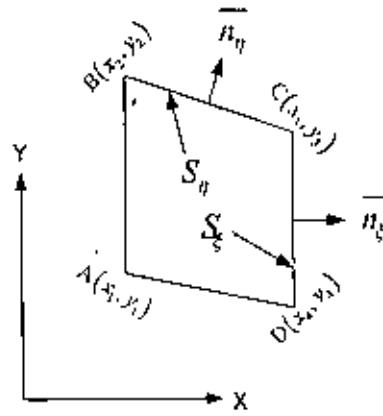


Fig. 2.5 Surface vectors in terms of components

It can be noted here that S_{ξ} , $S_{\xi'}$, S_{η} , $S_{\eta'}$ can never be negative since these represent real lengths in a physical domain. The magnitudes of these vectors are given by

$$\begin{aligned} |\overline{S_{\xi}}| &= \sqrt{S_{\xi_x}^2 + S_{\xi_y}^2} = S_{\xi} \\ |\overline{S_{\eta}}| &= \sqrt{S_{\eta_x}^2 + S_{\eta_y}^2} = S_{\eta} \end{aligned} \quad (2.1.13)$$

2.1.4 Area of the cell

The vector area of a quadrilateral is half the cross product of the diagonal vectors. The cell scalar area is equal to the one half of the magnitude of the outer product of the line vectors which link opposite vertices of the cell. Thus the scalar area of the cell shown in Fig.2.6 can be given by

$$dV = \frac{1}{2} \begin{vmatrix} x_3 - x_1 & y_3 - y_1 \\ x_2 - x_1 & y_2 - y_1 \end{vmatrix}$$

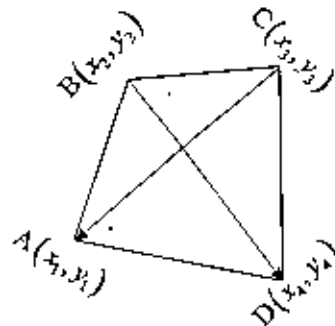


Fig. 2.6 Area of a typical cell

2.2 Discretization equations

Exact/Analytical solutions of some of the partial differential equations can be found which mainly involve closed-form expressions/function that give the continuous variation of the dependent variables within the domain of definition. In many instances, especially in most physical problems, either the exact solution can not be derived or is too cumbersome. In these situations, numerical solutions can be of great help. Numerical analysis can give values at discrete points in the domain, called grid points. In many Computational Fluid Dynamics (CFD) applications, involving numerical solutions uses uniformly spaced grids in a certain direction mainly because it can remarkably simplify the programming difficulties and can save memory spaces of the computer. The uniform spacing not necessarily has to happen in physical space due to the fact that the calculations are carried out in a transformed computational space which has uniform spacing. Discretization can be defined as the process of replacing the partial differential equations (PDEs) into a set of Algebraic equations thereby called Discretization equation.

Now in order to discretize eqn. (2.1.10), let's rewrite it with the help of eqns (2.1.11) & (2.1.12), as follows

$$\begin{aligned} \int_V \frac{\partial Q}{\partial t} dV + \int_{S_x} \left\{ \left[S_{\xi_x} (E - E_v) + S_{\xi_y} (F - F_v) \right] / S_{\xi} \right\} dS_{\xi} \\ + \int_{S_y} \left\{ \left[S_{\eta_x} (E - E_v) + S_{\eta_y} (F - F_v) \right] / S_{\eta} \right\} dS_{\eta} = 0 \end{aligned} \quad (2.2.1)$$

In eqn. (2.2.1), inviscid flux terms are written as $F_{\xi} = (S_{\xi_x} E + S_{\xi_y} F) / S_{\xi}$, $F_{\eta} = (S_{\eta_x} E + S_{\eta_y} F) / S_{\eta}$. Expanding it further, we have the details as given below

$$\begin{aligned} E_{\xi} &= (S_{\xi_x} E + S_{\xi_y} F) / S_{\xi} \\ &= \left\{ S_{\xi_x} \begin{bmatrix} \rho u \\ \rho u^2 + P \\ \rho uv \end{bmatrix} + S_{\xi_y} \begin{bmatrix} \rho v \\ \rho vu \\ \rho v^2 + P \end{bmatrix} \right\} \times \frac{1}{S_{\xi}} \end{aligned}$$

$$= \frac{1}{S_\xi} \begin{bmatrix} \rho(S_{\xi_x} u + S_{\xi_y} v) \\ \rho(S_{\xi_x} u^2 + S_{\xi_y} vu) + S_{\xi_x} P \\ \rho(S_{\xi_x} uv + S_{\xi_y} v^2) + S_{\xi_y} P \end{bmatrix}$$

$$\text{Therefore, } E_\xi = \begin{bmatrix} \rho u_\xi \\ \rho u u_\xi + P S_{\xi_x} / S_\xi \\ \rho v u_\xi + P S_{\xi_y} / S_\xi \end{bmatrix} \quad (2.2.2)$$

where contravariant u-component velocity u_ξ , is defined as $(S_{\xi_x} u + S_{\xi_y} v) / S_\xi$. Similarly,

$F_\eta = (S_{\eta_x} E + S_{\eta_y} F) / S_\eta$ can be written as

$$F_\eta = \begin{bmatrix} \rho v_\eta \\ \rho u v_\eta + P S_{\eta_x} / S_\eta \\ \rho v v_\eta + P S_{\eta_y} / S_\eta \end{bmatrix} \quad (2.2.3)$$

where the contravariant v-component velocity, v_η is defined as $(S_{\eta_x} u + S_{\eta_y} v) / S_\eta$. Now rewriting the contravariant velocities, we have

$$\begin{aligned} u_\xi &= (S_{\xi_x} u + S_{\xi_y} v) / S_\xi \\ v_\eta &= (S_{\eta_x} u + S_{\eta_y} v) / S_\eta \end{aligned} \quad (2.2.4)$$

Next, viscous fluxes have the notations E_{v_ξ}, F_{v_η} and can be written explicitly as given below:

$$\begin{aligned} E_{v_\xi} &= (S_{\xi_x} E_{v_\xi} + S_{\xi_y} F_{v_\xi}) / S_\xi \\ &= \frac{1}{S_\xi} \begin{bmatrix} 0 \\ S_{\xi_x} \tau_{xx} + S_{\xi_y} \tau_{yx} \\ S_{\xi_x} \tau_{xy} + S_{\xi_y} \tau_{yy} \end{bmatrix} \end{aligned} \quad (2.2.5)$$

$$F_{v_\eta} = (S_{\eta_x} E_v + S_{\eta_y} F_v) / S_\eta \quad (2.2.6)$$

$$= \frac{1}{S_\eta} \begin{bmatrix} 0 \\ S_{\eta_x} \tau_{xx} + S_{\eta_y} \tau_{yx} \\ S_{\eta_x} \tau_{xy} + S_{\eta_y} \tau_{yy} \end{bmatrix}$$

In the generalized coordinate, we can rewrite the conservation law as follows

$$\int_V \frac{\partial Q}{\partial t} dV + \int_{S_\xi} (E_\xi - E_{v_\xi}) dS_\xi + \int_{S_\eta} (F_\eta - F_{v_\eta}) dS_\eta = 0 \quad (2.2.7)$$

The notation and the symbols have already been defined previously. Now, we are going to derive the x components explicitly.

2.3 Discretization equation for u

The discretization of the integral equations is called finite volume (FV). In finite volume method, the conservation principles are applied to a fixed region in space known as control volume. Control Volume Method (CVM) will be used for our discretization purposes. CVM has been opted of other technique because it's not only a mathematical approximation; but also it has a clear physical significance. Discretization equations derived by CVM preserve the conservation law for the relevant property for each control volume and thereby over the whole calculation domain. Perfect overall balance of mass, energy and momentum can't be ensured by other methods. The key step of the finite volume method is the integration of the governing equation over a control volume to produce a discretize equations at its nodal point.

The x-component of the conservation equation

The x-component of the conservation equation (2.2.7) can be written as

$$\int_{S_\xi} \left[\rho u u_\xi + P S_{\xi_x} / S'_\xi - \frac{1}{S_\xi} (S_{\xi_x} \tau_{xx} + S_{\xi_y} \tau_{yx}) \right] dS_\xi + \int_{S_\eta} \left[\rho u u_\eta + P S_{\eta_x} / S_\eta - \frac{1}{S_\eta} (S_{\eta_x} \tau_{xx} + S_{\eta_y} \tau_{yx}) \right] dS_\eta = 0 \quad (2.3.1)$$

Now calculating the third term under the first integral, that is

$$\int_{S_\xi} (S_{\xi_x} \tau_{xx} + S_{\xi_y} \tau_{yx}) dS_\xi \quad (2.3.2)$$

Substituting τ_{xx} , τ_{yx} from eqns (2.1.4-5) into eqn (2.3.2), we have,

$$\begin{aligned}
 & \int_{S_\xi} \left[S_{\xi_x} \left(2\mu \frac{\partial u}{\partial x} - \frac{2}{3} \mu \nabla \cdot \vec{V} \right) + S_{\xi_y} \mu \left(\frac{\partial v}{\partial x} + \frac{\partial u}{\partial y} \right) \right] dS_\xi \\
 &= \int_{S_\xi} \mu \left(S_{\xi_x} \frac{\partial u}{\partial x} + S_{\xi_y} \frac{\partial u}{\partial y} \right) dS_\xi + \\
 & \underbrace{\int_{S_\xi} \left[\mu \left(S_{\xi_x} \frac{\partial u}{\partial x} + S_{\xi_y} \frac{\partial v}{\partial x} \right) - \frac{2}{3} \mu S_{\xi_x} (\nabla \cdot \vec{V}) \right] dS_\xi}_{\text{extra terms}} \tag{2.3.3}
 \end{aligned}$$

First of all, we are going to derive discretization equation for the incompressible flow, which means the equation without extra terms. The problem that we are involved has flow of incompressible type. Now the x-component of the incompressible flow from eqn (2.3.1) can be written as

$$\begin{aligned}
 & \int_{S_\xi} \left[\rho u u_\xi + P S_{\xi_x} / S_\xi - \frac{\mu}{S_\xi} \left(S_{\xi_x} \frac{\partial u}{\partial x} + S_{\xi_y} \frac{\partial u}{\partial y} \right) \right] dS_\xi + \\
 & \int_{S_\eta} \left[\rho u v_\eta + P S_{\eta_x} / S_\eta - \frac{\mu}{S_\eta} \left(S_{\eta_x} \frac{\partial u}{\partial x} + S_{\eta_y} \frac{\partial u}{\partial y} \right) \right] dS_\eta = 0 \tag{2.3.4}
 \end{aligned}$$

The numerical treatments of every term sequentially in order to implant those in the program are given next:

Discretization of the terms involving conservation of mass, i.e.,

$$\begin{aligned}
 & \int_{S_\xi} \rho u u_\xi dS_\xi + \int_{S_\eta} \rho u v_\eta dS_\eta \\
 &= (\rho u_\xi S_\xi)_e u_e - (\rho u_\xi S_\xi)_w u_w + (\rho v_\eta S_\eta)_n u_n - (\rho v_\eta S_\eta)_s u_s \tag{2.3.5} \\
 &= \left[\left(\rho \frac{CVX}{S_\xi} S_\xi \right)_e u_e - \left(\rho \frac{CVX}{S_\xi} S_\xi \right)_w u_w \right] \\
 & \quad + \left[\left(\rho \frac{CVE}{S_\eta} S_\eta \right)_n u_n - \left(\rho \frac{CVE}{S_\eta} S_\eta \right)_s u_s \right] \\
 &= [(\rho \cdot CVX)_e u_e - (\rho \cdot CVX)_w u_w] + [(\rho \cdot CVE)_n u_n - (\rho \cdot CVE)_s u_s]
 \end{aligned}$$

where,

$$CVX = S_{\xi} u + S_{\xi_y} v$$

$$CVE = S_{\eta} u + S_{\eta_y} v$$

Discretization of the pressure terms

$$\begin{aligned} & \int_{S_{\xi}} P \frac{S_{\xi_x}}{S_{\xi}} dS_{\xi} + \int_{S_{\eta}} P \frac{S_{\eta_x}}{S_{\eta}} dS_{\eta} \\ &= (PS_{\xi_x})_e - (PS_{\xi_x})_w + (PS_{\eta_x})_n - (PS_{\eta_x})_s \\ \therefore dpdx &= P_e (S_{\xi_x})_e - P_w (S_{\xi_x})_w + P_n (S_{\eta_x})_n - P_s (S_{\eta_x})_s \end{aligned} \quad (2.3.6)$$

Discretization of terms involving u velocity gradients over the ξ surface, i.e.,

$$= \int_{S_{\xi}} \frac{\mu}{S_{\xi}} \left(S_{\xi_x} \frac{\partial u}{\partial x} + S_{\xi_y} \frac{\partial u}{\partial y} \right) dS_{\xi} \quad (2.3.7)$$

We first discretize the velocity involving term. Applying an alternate form of the Gauss Divergence Theorem followed by the utilization of the integral definition of divergence, we can approximate the derivative as follows:

$$\begin{aligned} \frac{\partial u}{\partial x} &\rightarrow \frac{1}{\Delta V} \int_V \frac{\partial u}{\partial x} dV = \frac{1}{\Delta V} \int_S u \hat{i} \cdot \vec{n} dS \\ &= \frac{1}{\Delta V} \left[\int_{S_{\xi}} u \frac{S_{\xi_x}}{S_{\xi}} dS_{\xi} + \int_{S_{\eta}} u \frac{S_{\eta_x}}{S_{\eta}} dS_{\eta} \right] \\ &= \frac{1}{\Delta V} \left[\left(u \frac{S_{\xi_x}}{S_{\xi}} S_{\xi} \right)_e - \left(u \frac{S_{\xi_x}}{S_{\xi}} S_{\xi} \right)_w + \left(u \frac{S_{\eta_x}}{S_{\eta}} S_{\eta} \right)_n - \left(u \frac{S_{\eta_x}}{S_{\eta}} S_{\eta} \right)_s \right] \\ \therefore \frac{\partial u}{\partial x} &= \frac{1}{\Delta V} [S_{\xi_x} (u_e - u_w) + S_{\eta_x} (u_n - u_s)] \end{aligned} \quad (2.3.8)$$

where $(S_{\xi_x})_e = (S_{\xi_x})_w = S_{\xi_x}$, $(S_{\eta_x})_n = (S_{\eta_x})_s = S_{\eta_x}$, dV is the volume element enclosed by the surface S and \vec{n} is the outward drawn normal to the surface S and is given by eqn (2.1.12).

Applying exactly similar steps, we have

$$\frac{\partial u}{\partial y} = \frac{1}{\Delta V} \left[S_{\xi_y} (u_e - u_w) + S_{\eta_y} (u_n - u_s) \right] \quad (2.3.9)$$

From eqn (2.3.7), we have

$$\int_{S_\xi} \frac{\mu}{S_\xi} \left(S_{\xi_x} \frac{\partial u}{\partial x} + S_{\xi_y} \frac{\partial u}{\partial y} \right) dS_\xi = \mu \left[\int_{S_\xi} \frac{1}{S_\xi} S_{\xi_x} \frac{\partial u}{\partial x} dS_\xi + \int_{S_\xi} \frac{1}{S_\xi} S_{\xi_y} \frac{\partial u}{\partial y} dS_\xi \right]$$

Substituting eqns (2.3.8) & (2.3.9) into the above eqn we have

$$\begin{aligned} & \int_{S_\xi} \frac{\mu}{S_\xi} \left[S_{\xi_x} \frac{1}{dV} \left\{ (u_e - u_w) S_{\xi_x} + (u_n - u_s) S_{\eta_x} \right\} \right. \\ & \quad \left. + S_{\xi_y} \frac{1}{dV} \left\{ (u_e - u_w) S_{\xi_y} + (u_n - u_s) S_{\eta_y} \right\} \right] dS_\xi \\ & = \int_{S_\xi} \frac{\mu}{S_\xi} \frac{1}{dV} \left[(S_{\xi_x}^2 + S_{\xi_y}^2) (u_e - u_w) + (S_{\xi_x} S_{\eta_x} + S_{\xi_y} S_{\eta_y}) (u_n - u_s) \right] dS_\xi \end{aligned}$$

Now performing the integration, keeping in mind that upper case letters denote grid points and lower case letters denote the interface of the CV as shown in Fig. 2.7, we have

$$\begin{aligned} & = \left\{ \frac{\mu}{dV} (S_{\xi_x}^2 + S_{\xi_y}^2) \right\}_e (u_e - u_w) - \left\{ \frac{\mu}{dV} (S_{\xi_x}^2 + S_{\xi_y}^2) \right\}_w (u_w - u_e) \\ & + \left\{ \frac{\mu}{dV} (S_{\xi_x} S_{\eta_x} + S_{\xi_y} S_{\eta_y}) \right\}_e (u_n - u_s) - \left\{ \frac{\mu}{dV} (S_{\xi_x} S_{\eta_x} + S_{\xi_y} S_{\eta_y}) \right\}_w (u_n - u_s) \end{aligned}$$

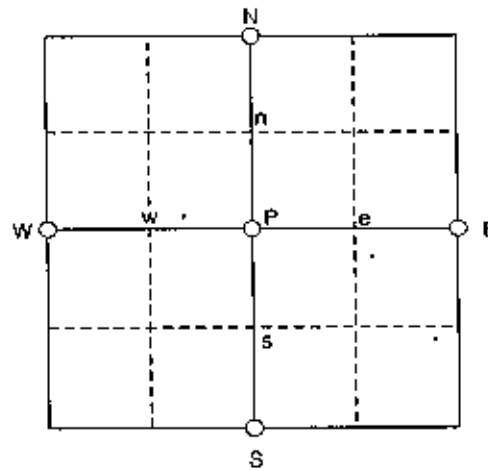


Fig. 2.7 An internal control volume with interior grid point P along with four neighbors

$$\begin{aligned} \text{Therefore, } \int_{S_\xi} \frac{\mu}{S_\xi} \left(S_{\xi_x} \frac{\partial u}{\partial x} + S_{\xi_y} \frac{\partial u}{\partial y} \right) dS_\xi \\ = D_e (u_e - u_p) - D_w (u_p - u_w) + C_e (u_n - u_s)_e - C_w (u_n - u_s)_w \end{aligned} \quad (2.3.10)$$

where

$$D_e = \left\{ \frac{\mu}{dV} (S_{\xi_x}^2 + S_{\xi_y}^2) \right\}_e = a_{\mu e}, \quad D_w = \left\{ \frac{\mu}{dV} (S_{\xi_x}^2 + S_{\xi_y}^2) \right\}_w = a_{\mu w} \quad (2.3.11)$$

$$C_e = \left\{ \frac{\mu}{dV} (S_{\xi_x} S_{\eta_x} + S_{\xi_y} S_{\eta_y}) \right\}_e, \quad C_w = \left\{ \frac{\mu}{dV} (S_{\xi_x} S_{\eta_x} + S_{\xi_y} S_{\eta_y}) \right\}_w \quad (2.3.12)$$

Discretization of the u velocity gradient terms over the η surface,

$$\begin{aligned} \int_{S_\eta} \frac{\mu}{S_\eta} \left(S_{\eta_x} \frac{\partial u}{\partial x} + S_{\eta_y} \frac{\partial u}{\partial y} \right) dS_\eta \\ = \int_{S_e} \frac{\mu}{S_\eta} S_{\eta_x} \frac{\partial u}{\partial x} dS_\eta + \int_{S_s} \frac{\mu}{S_\eta} S_{\eta_y} \frac{\partial u}{\partial y} dS_\eta \end{aligned} \quad (2.3.13)$$

Again substituting eqns (2.3.10) & (2.3.11) into the above eqn (2.3.13), we have,

$$\begin{aligned} \int_{S_\eta} \frac{\mu}{S_\eta} \left[\begin{aligned} & S_{\eta_x} \cdot \frac{1}{dV} \{ (u_e - u_w) S_{\xi_x} + (u_n - u_s) S_{\eta_x} \} \\ & + S_{\eta_y} \cdot \frac{1}{dV} \{ (u_e - u_w) S_{\xi_y} + (u_n - u_s) S_{\eta_y} \} \end{aligned} \right] dS_\eta \\ = \int_{S_p} \frac{\mu}{S_\eta} \cdot \frac{1}{dV} \left[(S_{\eta_x} S_{\xi_x} + S_{\eta_y} S_{\xi_y}) (u_e - u_w) + (S_{\xi_x}^2 + S_{\xi_y}^2) (u_n - u_s) \right] dS_\eta \\ = \left\{ \frac{\mu}{dV} (S_{\eta_x} S_{\xi_x} + S_{\eta_y} S_{\xi_y}) \right\}_n (u_e - u_w)_n - \left\{ \frac{\mu}{dV} (S_{\eta_x} S_{\xi_x} + S_{\eta_y} S_{\xi_y}) \right\}_s (u_e - u_w)_s \\ + \left\{ \frac{\mu}{dV} (S_{\eta_x}^2 + S_{\eta_y}^2) \right\}_n (u_n - u_p)_n - \left\{ \frac{\mu}{dV} (S_{\eta_x}^2 + S_{\eta_y}^2) \right\}_s (u_p - u_s)_s \end{aligned}$$

$$\begin{aligned} \text{Finally, } \int_{S_\eta} \frac{\mu}{S_\eta} \left(S_{\eta_x} \frac{\partial u}{\partial x} + S_{\eta_y} \frac{\partial u}{\partial y} \right) dS_\eta \\ = C_n (u_e - u_w)_n - C_s (u_e - u_w)_s + D_n (u_n - u_p)_n - D_s (u_p - u_s)_s \end{aligned} \quad (2.3.14)$$

where

$$D_n = \left\{ \frac{\mu}{dV} (S_{n_e}^2 + S_{n_s}^2) \right\}_n = a_n, \quad D_s = \left\{ \frac{\mu}{dV} (S_{n_e}^2 + S_{n_s}^2) \right\}_s = a_s \quad (2.3.15)$$

$$C_n = \left\{ \frac{\mu}{dV} (S_{n_e} S_{\xi_e} + S_{n_s} S_{\xi_s}) \right\}_n, \quad C_s = \left\{ \frac{\mu}{dV} (S_{n_e} S_{\xi_e} + S_{n_s} S_{\xi_s}) \right\}_s \quad (2.3.16)$$

With the help of eqns (2.3.5), (2.3.6), (2.3.12) & (2.3.14), eqn. (2.3.4) reduces to

$$a_p u_p = a_E u_E + a_W u_W + a_N u_N + a_S u_S + S_u \quad (2.3.17)$$

where

$$a_E = D_e = \left\{ \frac{\mu}{dV} (S_{\xi_e}^2 + S_{\xi_s}^2) \right\}_e$$

$$a_W = D_w = \left\{ \frac{\mu}{dV} (S_{\xi_e}^2 + S_{\xi_s}^2) \right\}_w$$

$$a_N = D_n = \left\{ \frac{\mu}{dV} (S_{n_e}^2 + S_{n_s}^2) \right\}_n$$

$$a_S = D_s = \left\{ \frac{\mu}{dV} (S_{n_e}^2 + S_{n_s}^2) \right\}_s$$

$$a_p = a_E + a_W + a_N + a_S - S_p$$

and S_u is the source term given by $S_u = S_w + S_p u_p$ with $S_w = cp * u(n) - dpdx$,

$S_p = -cp = -\text{Max}[0, smp]$ and smp is the net outflow from the control volume (mass source).

Here S_p represents all the terms those can not be approximated by values of u at the five points E, W, N, S and P.

2.4 Discretization equation for v

Now, we want to derive the discretization equation for v . In order to do that, we have to calculate the y-components of the N-S equations just as we did calculated the x-component while deriving the discretization equation for u . For the sake of brevity, we are presenting the final form of the discretized equation. Therefore, the final discretization equation for v can be written as

$$a_p v_p = a_E v_E + a_W v_W + a_N v_N + a_S v_S + S_v \quad (2.4.1)$$

where

$$\begin{aligned}
 a_E = D_e &= \left\{ \frac{\mu}{d^3 \nabla} (S_{e_x}^2 + S_{e_y}^2) \right\}_e \\
 a_W = D_w &= \left\{ \frac{\mu}{d^3 \nabla} (S_{w_x}^2 + S_{w_y}^2) \right\}_w \\
 a_N = D_n &= \left\{ \frac{\mu}{d^3 \nabla} (S_{n_x}^2 + S_{n_y}^2) \right\}_n \\
 a_S = D_s &= \left\{ \frac{\mu}{d^3 \nabla} (S_{s_x}^2 + S_{s_y}^2) \right\}_s \\
 a_P &= a_E + a_W + a_N + a_S - S_P
 \end{aligned}$$

where S_v is the source term given by $S_v = S_{v_x} + S_{v_y} \nu_\nu$, $S_{v_x} = cp^* v(n) - dp/dx$, S_{v_y} represents all the terms those can not be approximated by values of v at the five points E, W, N, S and P. All other symbols and notations used in this section have logically similar form and conventional meaning as that of u defined in the earlier section of the same chapter.

2.5 Discretization of the energy equation

The energy equation for an incompressible flow having constant properties is decoupled from the continuity and momentum equations. Therefore, the energy equation can be solved subsequent to the computation of the velocity field to provide the temperature distribution.

For Newtonian fluid without any heat generation and having constant properties along with the Fourier heat conduction law and for a two-dimensional incompressible flow, the conservative form of the energy equation is expressed as

$$\rho c_p \left[\frac{\partial T}{\partial t} + \frac{\partial}{\partial x} (uT) + \frac{\partial}{\partial y} (vT) \right] = k \nabla^2 T + \mu \phi \quad (2.5.1)$$

where k is the thermal conductivity and μ is the viscosity and ϕ denote the viscous dissipation term given by

$$\phi = 2 \left[\left(\frac{\partial u}{\partial x} \right)^2 + \left(\frac{\partial v}{\partial y} \right)^2 \right] + \left(\frac{\partial u}{\partial y} + \frac{\partial v}{\partial x} \right)^2 \quad (2.5.2)$$

For laminar-boundary layer, eqn. (2.5.1) can equivalently be written as follows

$$\frac{\partial T}{\partial t} + u \frac{\partial T}{\partial x} + v \frac{\partial T}{\partial y} = \alpha \nabla^2 T \quad (2.5.3)$$

where α and ν are the thermal diffusivity and the kinematic viscosity given by

$$\alpha = \frac{k}{\rho c_p}, \quad \nu = \frac{\mu}{\rho} \quad (2.5.4)$$

In dimensionless form, energy equation can be written as

$$\frac{\partial T}{\partial t} + u \frac{\partial T}{\partial x} + v \frac{\partial T}{\partial y} = \frac{1}{Pr Re} \left(\frac{\partial^2 T}{\partial x^2} + \frac{\partial^2 T}{\partial y^2} \right) \quad (2.5.5)$$

where Re is the Reynolds number and Pr is the Prandtl number and are given by

$$Pr = \frac{\nu}{\alpha} = \frac{\mu c_p}{k} \quad (2.5.6)$$

It is evident that the energy equation is linear. Therefore, the procedure described previously for solving the momentum equation can also be utilized to solve the energy equation. Hence, the discretized final equation is presented next

$$a_p T_p = a_E T_E + a_W T_W + a_N T_N + a_S T_S + S_i \quad (2.5.7)$$

where

$$a_E = \left\{ \frac{\mu}{prl \times d \nabla} (S_{\xi'}^2 + S_{\xi''}^2) \right\}_e$$

$$a_W = \left\{ \frac{\mu}{prl \times d \nabla} (S_{\xi'}^2 + S_{\xi''}^2) \right\}_w$$

$$a_N = \left\{ \frac{\mu}{prt \times d^2} (S_{n_x}^2 + S_{n_y}^2) \right\}_n$$

$$a_S = \left\{ \frac{\mu}{prt \times d^2} (S_{n_x}^2 + S_{n_y}^2) \right\}_s$$

$$a_p = a_E + a_W + a_N + a_S - S_p$$

$$S_p = cp \times t(n)$$

Here prt is the laminar Prandtl number and cp has the identical representation as defined for u and v . Here, S_t is the source term given by $S_t = S_v + S_p t_p$, S_p represents all the terms those can not be approximated by values of t at the five points E, W, N, S and P. All other symbols and notations used in this section have logically similar form and conventional meaning as those of u and v defined in the earlier sections of the same chapter. All the calculation steps involved in solving the N-S equations in non-orthogonal generalized coordinate can be visualized shortly with the help of the flowchart. The flowchart for the computation of the flow field and the temperature distribution using a non-orthogonal generalized coordinates system has been shown in Fig 2.8.next.

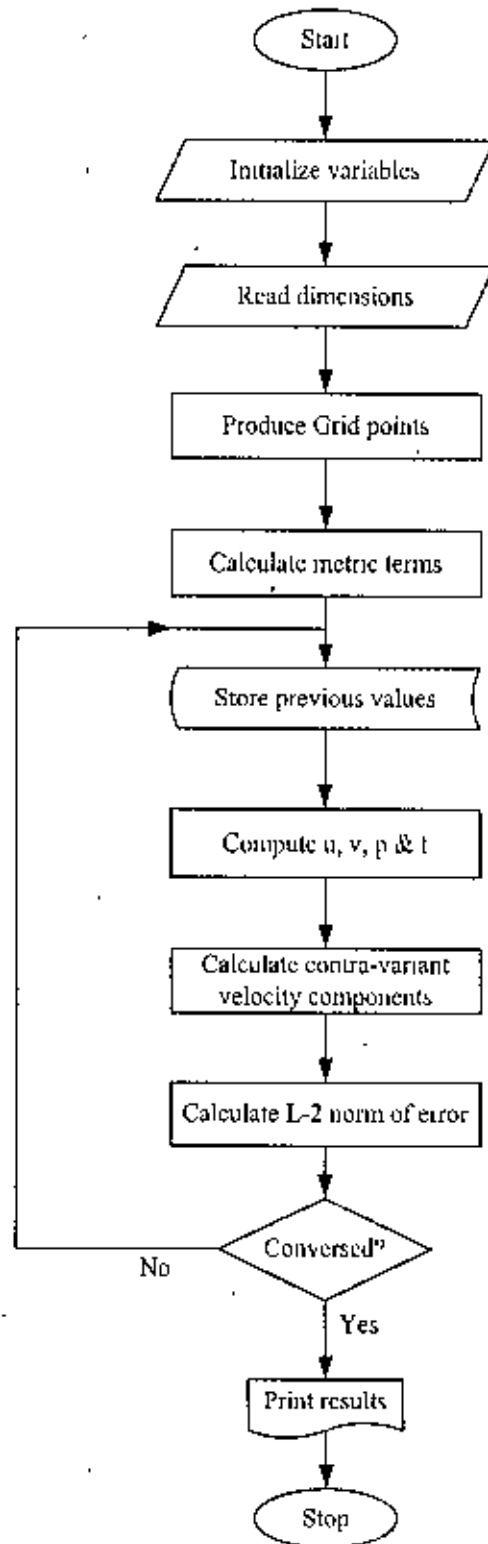


Fig. 2.8 Flowchart of the program based on generalized non-orthogonal coordinate

2.6 Relaxation and convergence criteria

Numerical methods used to solve the equations for fluid flow and heat transfer most often employ one or more iteration procedures. The iterative solution methods require convergence criteria that are used to decide when the iterations can be terminated. In the program code, we used L-2 norm of error as a convergence criterion defined below:

$$\text{Max} \left[\sqrt{\frac{(\phi(n) - \phi_{\text{old}}(n))^2}{\phi_{\text{old}}(n)}} \right] \leq 10^{-6}$$

No. of grid points

Here $\phi(n)$ & $\phi_{\text{old}}(n)$ are the values of the dependent variable at the current and previous steps/iterations respectively.

2.7 Pressure equation; Pressure based algorithm-SIMPLE

The existing algorithms to solve the Navier-Stokes equations can be generally classified as density-based methods and pressure-based methods. For these methods, the velocity field is normally specified using the momentum equations. The pressure based methods, initially developed for incompressible flow regimes, obtain the pressure field via a pressure or a pressure correction equation which is formulated by manipulating the continuity and momentum equations [23]. The solution procedure is conventionally sequential in nature. The pressure-based methods can be extended to compressible flows by taking the dependence of density on pressure, via the equation of state, into account. More details in this respect can be found from [23-24].

2.8 Code validation

The developed FORTRAN source codes need to be validated through reproducing the published results in identical working/boundary conditions. A typical problem that has wall boundaries surrounding the whole computational domain is the driven cavity problem as illustrated in Fig. 2.9. In the shown squared cavity, the incompressible viscous flow is driven by the uniform translation of the upper lid. The lid-driven cavity flow has been playing as an enriched source for pioneering research in CFD. Thus far, cavity flow is an area of con-

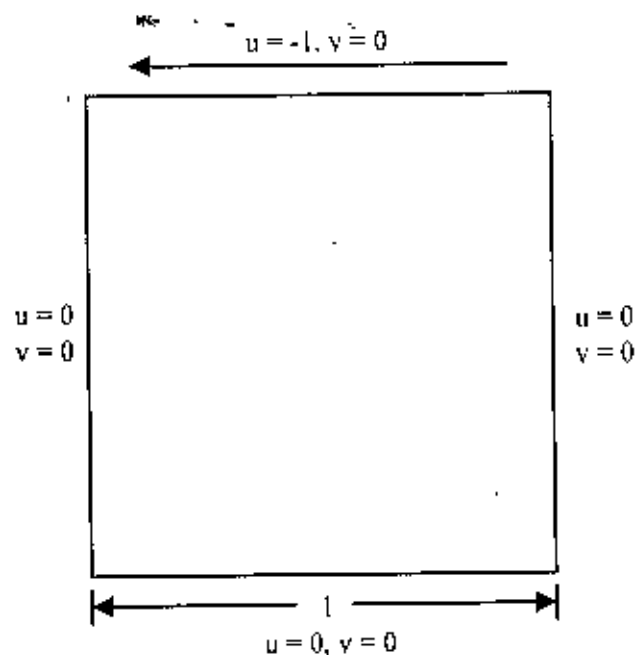


Fig. 2.9 A lid driven square cavity along with boundary conditions

timing interest and was regarded as a benchmark study in some major works. The geometrical simplicity of the cavity facilitates experimental calibrations or numerical implementations, thus providing benchmark data for comparison and validation. However, the flow physics inside the cavity is by no means simple. Comprehensive numerical investigation of the flow physics inside a lid-driven cavity for various Reynolds numbers (Re) have been done by several researchers. The availability of the accurate numerical solutions for the lid-driven cavity flow established itself as the benchmark for the assessment of numerical methods and the validation of Navier–Stokes codes. In this section, we are going to validate the applicability of the developed model FORTARN code in simulating the steady base flow within a lid-driven cavity by carrying out a comparison test. In the absence of body forces, the dimensionless equations have the following tensor form for a given Re :

$$\frac{\partial u_i}{\partial x_i} = 0$$

$$\frac{\partial}{\partial x_j} (u_i u_j) = -\frac{\partial p}{\partial x_i} + \frac{1}{Re} \frac{\partial^2 u_i}{\partial x_j^2}$$

where $i, j = 1, 2$ corresponds to $x(u), y(v)$ coordinates(velocities) in two-dimensions respectively, p is the static pressure and Re is the Reynolds number defined by $Re = U_0 D/\nu$, where ν is the kinematic viscosity. In Fig. 2.9, D , the height/width of the squared cavity, and lid-driven velocity, U_0 , are specified as the unit length and velocity respectively. Boundary conditions for the velocity field are the lid-driven unit velocity at the top-wall and no-slip conditions for velocity components at all the rest walls. These are given by

$$\begin{aligned} u &= -1, \quad v = 0; \quad y = 1 \\ u = v &= 0; \quad x = y = 0, \quad x = 1 \end{aligned}$$

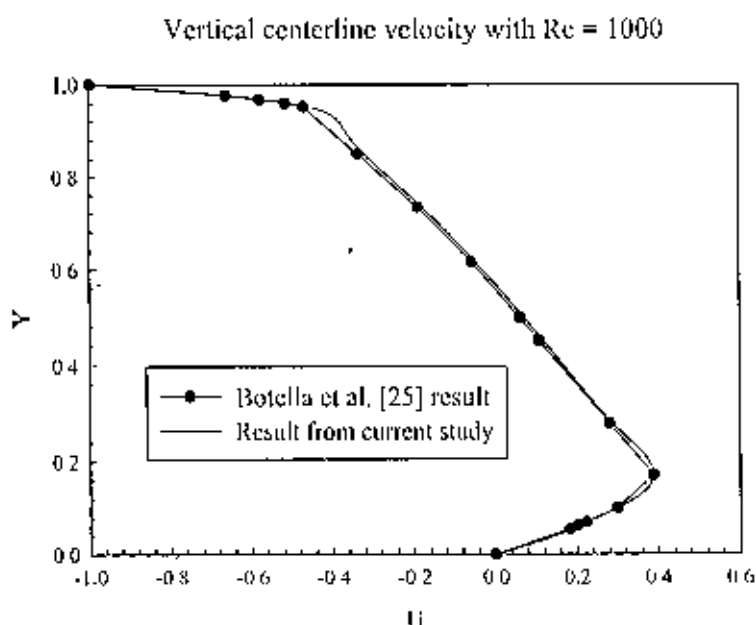


Fig. 2.10 Comparative u -velocity at vertical centerline of the cavity

$Re = 1000$ is frequently chosen as a standard test condition as we do here as well, for the comparison of the results obtained from different methods/schemes. Two-dimensional numerical results are available from numerous sources. Now we are presenting the velocity profiles only at the vertical centerline is shown in Fig. 2.10. From figure 2.10, it can be claimed that the result obtained from our model codes match very well with that of Botella [25].

2.9 Conclusion

The basic equation in conservative form has been derived in this chapter using generalized non-orthogonal coordinate system. The equations were then discretized using the finite volume method utilizing the non-staggered grids. Momentum equation was solved using the hybrid scheme. SIMPLE algorithm was used to handle the pressure-velocity coupling. The codes were verified with the published results and found to produce satisfactory results when applied to the lid driven cavity flow. Flow characteristics and the heat transfer inside the HCCCT is investigated at the third chapter.

Chapter Three

Numerical simulation of the hybrid closed circuit cooling tower

3.1 Introduction

CFD can facilitate better and faster design and analysis of the HCCCT, which could lead to shorter design cycles. Therefore time, money and energy can be saved substantially. Selecting the best designed HCCCT based on the optimum performance from the numerical analysis, equipment improvements could be built and installed with minimal downtime.

3.2 Numerical study of the cooling tower in dry mode

The thermal capacities and the flows inside the cooling towers are function of complex heat and mass transfer phenomenon among three fluids: the process fluid within the tube bundles, the spray water and the air. The highly complex nature of the relationships has made accurate performance prediction virtually impossible based on simple analysis. To keep the task as simple as possible without sacrificing the generality, the whole simulating works can be broadly divided into two main categories namely the characteristics based on the dry mode operation and that of the operation based on wet mode. For the dry mode operation, the performance characteristics of HCCCT having a rated capacity of 2 RT are investigated next.

3.2.1 Simulation of the HCCCT having a rated capacity of 2 RT

The schematic of the HCCCT is shown in Fig 3.1. Table 3.1 shows the geometrical parameters used in this simulation. Table 3.2 shows the basic/initial operating condition in order for deriving the proper operating condition to select the best performance of the HCCCT.

Table 3.1 Geometric parameters of the 2 RT HCCCT

Length of the heat exchanger	[m]	0.7
Width of the heat exchanger	[m]	0.65
Height of the heat exchanger	[m]	1.12
Number of coils at heat exchanger	[-]	16×7

Table 3.2 Simulation condition for the 2 RT HCCCT

Process fluid	Mass flow rate	[kg/h]	1000 ~ 1700
	Inlet temperature	[$^{\circ}$ C]	37
Spray water	Mass flow rate	[kg/h]	1600 ~ 2500
Air	Velocity	[m/s]	1.5 ~ 4.0
	Inlet wet-bulb temperature	[$^{\circ}$ C]	15 ~ 32

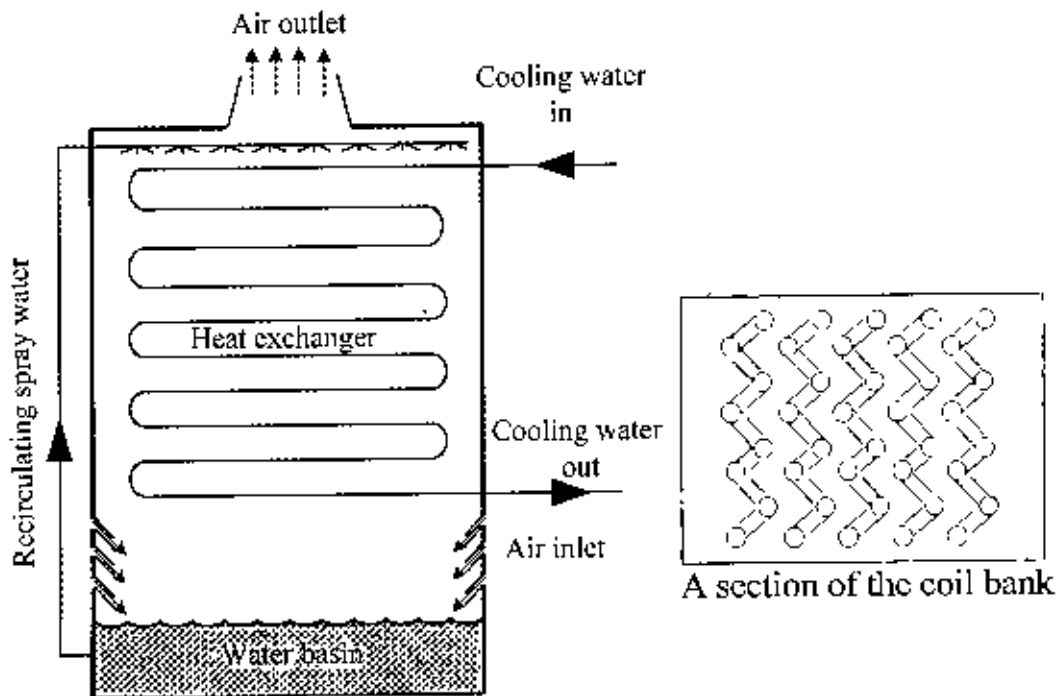


Fig. 3.1 Schematic of the HCCCT

3.2.2 The flow characteristics inside HCCCT with a capacity of 2 RT

The internal flow behavior is being checked in this section starting with the velocity vectors. The inlet is located at the bottom end of the tower and three passes are used for forcing the air into the tower. Fig. 3.2 gives the velocity vector's pattern where the right one gives a magnified view of the predicted air flow through the heat exchanger. The velocity of the air was found to be higher around the air inlet and several turbulences have been formed

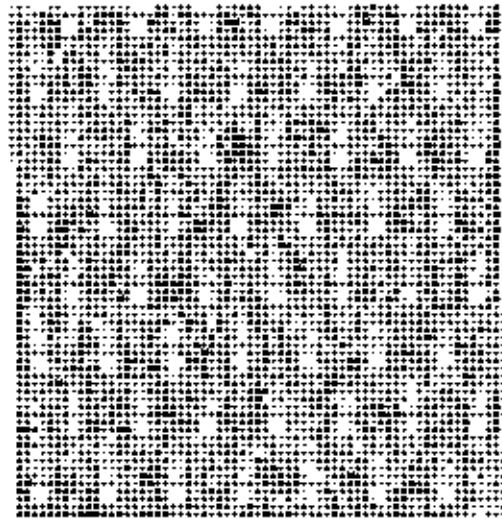


Fig. 3.2 Velocity vector inside 2 RT HCCCT

over there. The predicted air flow at the bottom part of the tower is seen to be a bit non uniform but as the flow approaches the heat exchanger, it gets more and more uniform and right at coil bank, it could be claimed that the air flow is uniform.

3.2.3 Temperature distribution in 2 RT tower w.r.t. air inlet velocity

In dry mode, only air is used from the bottom to cool the coils and the velocity of the air plays an important role both for the pressure drop and cooling capacity. We checked the influence of the air velocity for 4 different cases namely for an inlet velocity of 1.5, 2, 2.75 and 3 m/s. The temperature of the cooling water is seen to decrease with the increase of the air velocity. In the simulation, a constant air temperature of 15°C and a constant cooling water temperature of 37°C were used for all the cases with a cooling water mass flow rate of 1600 kg/h. A comparative temperature distribution along the coil height is given in Fig. 3.3. The row number 16 in Fig. 3.3 implies the highest elevation of the heat exchanger and row 1 means the lowest part of the coil bank. The temperature of the cooling water is seen to decrease almost linearly for the increase of the air velocity and for the highest air velocity of 3 m/s, the temperature drop is the highest which is about 1.48°C and at a simulation condition of 2.75 m/s, the temperature drop is 1.37°C . Therefore, the cooling capacity of the 2 RT HCCCT is about 2192 kcal/h.

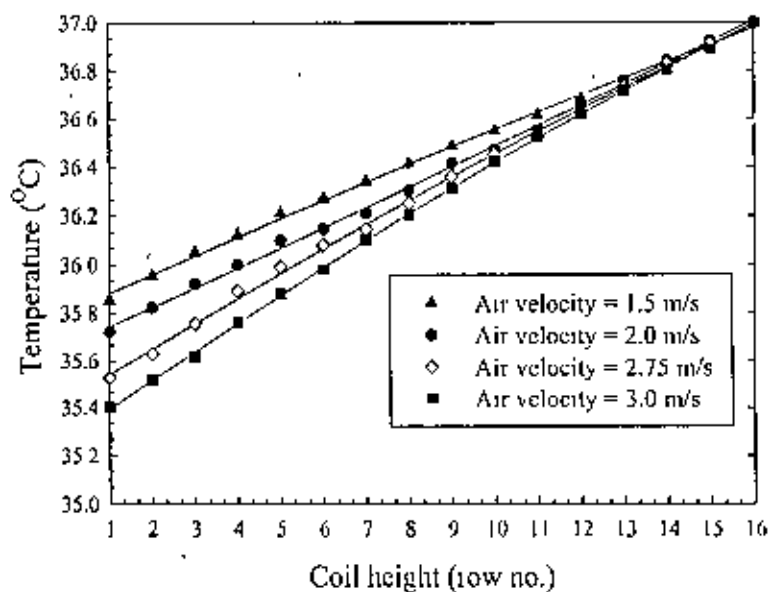


Fig. 3.3 Temperature distribution w.r.t. air inlet velocity

3.2.4 Temperature drop w.r.t. cooling water inlet temperature

The cooling water inlet temperature can bring notable difference in the cooling capacity. The influences of the cooling water inlet temperature for 5 different cases of 30, 35, 37, 40 and 43°C have been investigated. This time, a constant inlet air temperature of 15°C and a

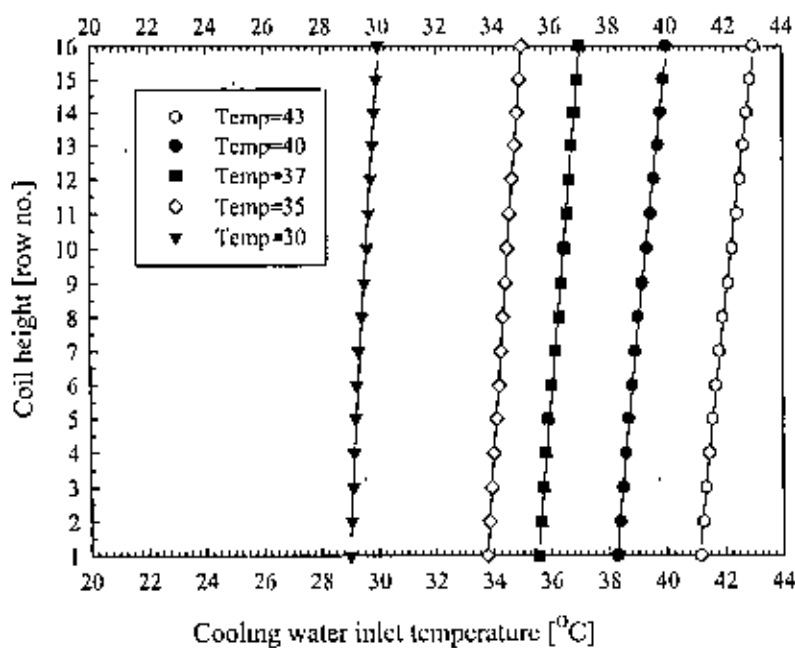


Fig. 3.4 Temperature drop w.r.t. cooling water inlet temperature.

constant cooling water mass flow rate of 1600 kg/h were used. The temperature is seen to decrease more rapidly for the cooling water having higher inlet temperature. A comparative temperature distribution along the coil height is shown in Fig. 3.4. The temperature is seen to decrease almost linearly. The temperature drop, which is calculated subtracting the temperature of the lowest coil from that of the top most coil, is seen to be higher for the cooling water having temperature of 43°C. Although the higher cooling effect can be obtained having high inlet cooling water temperature but the outlet cooling water temperature is also high for higher inlet cooling water temperature which is undesirable. At the simulation condition of 37°C, the temperature drop is 1.35°C. Therefore, the cooling capacity is about 2160 kcal/h.

3.2.5 Temperature drop with respect to air inlet temperature

The air inlet temperature can influence the cooling capacity. The impact is especially noteworthy for the dry mode operation of the HCCCT. The influences of the air inlet temperature for 4 different cases of 5, 10, 12, and 15°C have been studied. A comparative temperature distribution along the coil height is given in Fig. 3.5. The temperature is seen to decrease almost linearly along the coil height. The temperature drop is seen to be higher for the lower air inlet temperature. At the simulation condition of 15°C, the temperature drop is 1.37°C. The cooling capacity is about 2192 kcal/h.

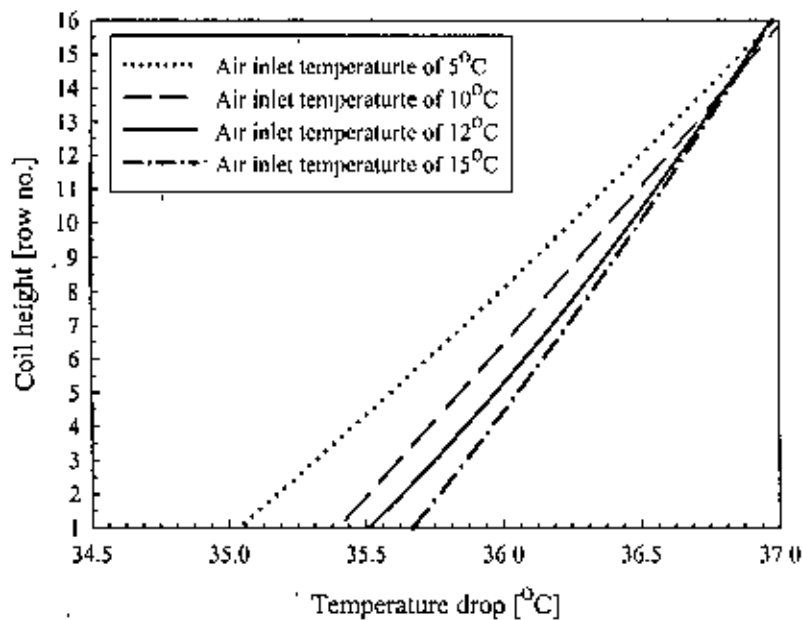


Fig. 3.5 Temperature distribution w.r.t. air inlet temperature

3.2.6 Pressure drop due to different arrangement of coil pitch having the air inlet at the side wall

The coil pitch plays a very important role for raising the heat transfer brought about by the passing air and water flow through heat exchanger in a ICCCT. Too small spacing between the coils can reduce the velocity of the air and water and thereby the heat transfer efficiency can be lower as well. Especially, at the air side, more pressure drop causes even more power requirement by the fan. Pressure drops decreased with the increase of the coil's transverse pitches as expected. For 32, 40, and 45 mm pitches, the air velocities at the inlet were maintained to remain constant at 3.1 m/s. From Fig. 3.6, it is clear that the coils having higher pitch has lower pressure drop and vice versa and that all three cases has similar pressure at the lowest coil due to the constant inlet air flow rate. Coil having a transverse pitch of 45 mm produced lower pressure drop which was about 2.05 mmAq. Increasing the pitches are not a wise idea only for the sake of reducing the pressure drop because minimizing the pressure drop and the flow rate of the fluids can minimize the operating cost but it can maximize the size of the heat exchanger and thus the initial cost.

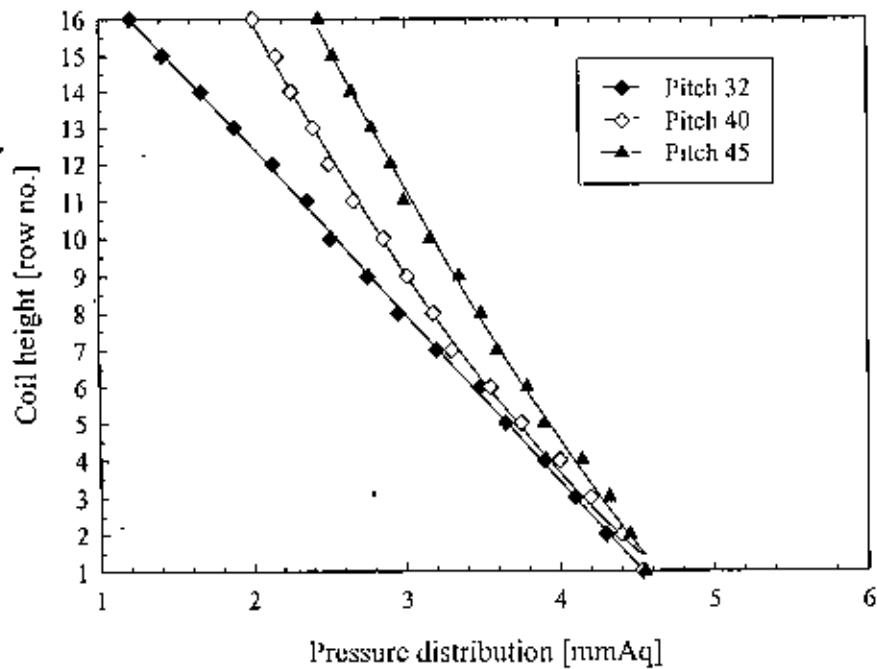


Fig. 3.6 Pressure distribution with respect to the coil pitch

3.3 Numerical Study of the wet closed cooling tower

The performance of the HCCCT for the wet mode operation during the summer is investigated in this section. The air flow is solved as a continuous phase using the Eulerian approach whereas the droplet trajectories are solved as the dispersed phase using the Lagrangian approach. The gas phase flow has already been solved in the previous section and now the water droplet trajectory equations as are being handled.

Water droplets trajectory equation

In wet mode operation, the spherical water droplets disseminate in the continuous gas phase. The particle trajectories are solved as the dispersed phase using the Lagrangian approach. The numerical simulation here has been designed to compute the velocity and the trajectories of the dispersed droplets. Utilizing the force balance on the droplet, the trajectory of a dispersed phase water droplet is predicted. Gan et al. [10] has reported a numerical technique for evaluating the performance of a closed wet cooling tower for the two-phase flow of gas and water droplets and they have shown that the equation of motion for a spherical water droplet which relates the velocity to the trajectory can be given by

$$\frac{dr_p}{dt} = V_p \quad (3.1)$$

where r_p is the trajectory and V_p is the instantaneous velocity of the droplet (m/s). The droplet velocity is obtained from the force balance. The force balance relates the droplet inertia to the forces acting on the droplet including the drag force, the buoyancy force, the force needed to accelerate the apparent mass of the droplet relative to gas and the force due to the pressure gradient in the gas surrounding the droplet. The droplet velocity, V_p can be written as

$$\rho_p \frac{dV_p}{dt} = \frac{3}{4} \frac{\rho C_D |V - V_p|}{d_p} (V - V_p) + g(\rho_p - \rho) + \frac{1}{2} \rho \frac{d}{dt} (V - V_p) + \frac{\partial P}{\partial r_p} \quad (3.2)$$

where V is the instantaneous local velocity of air (m/s), C_D is the drag coefficient, d_p is the droplet diameter (m), ρ_p is the droplet density (kg/m³) and P is the static pressure of gas (Pa). C_D , the drag coefficient, is a function of the relative Reynolds number given by:

$$C_D = a_1 + a_2/Re + a_3/Re^2 \quad (3.3)$$

where a_1 , a_2 and a_3 are constants which apply over several ranges of relative Reynolds number Re . The relative Reynolds number is defined as

$$Re = \frac{\rho d_p |V - V_p|}{\mu} \quad (3.4)$$

Here μ is the molecular viscosity of gas (kg/ms). The water droplet trajectory inside HCCCT is affected by the turbulent air flows, the effect is simulated using a stochastic droplet tracking method. In this method, the instantaneous gas phase velocity is decomposed into a mean and fluctuating component given by

$$V = \bar{V} + V' \quad (3.5)$$

\bar{V} , the mean gas velocity is determined solving the air phase continuous flow defined earlier. The fluctuating velocity V' is sampled randomly from a Gaussian probability distribution of the gas phase velocity. For an isotropic turbulent flow, it is given by

$$V' = \zeta \sqrt{\frac{2k}{3}} r_0 \quad (3.6)$$

where ζ is a normally distributed random number, k is the turbulent kinetic energy (m²/s²) and r_0 is a unit vector. The normal distribution is applied for the characteristic life-time of the gas eddy, defined as

$$\tau = \frac{C_\mu^{3/4} k}{\sqrt{2} \varepsilon} \quad (3.7)$$

where ε is the dissipation rate (m^2/s^3). The momentum transfer from the continuous phase to the dispersed phase is equal to the change in momentum of droplets passing through each control volume as follows

$$F = \sum \frac{3C_D \rho |V_p - V|}{4\rho_p d_p^2} (V_p - V) \dot{m}_p \Delta t \quad (3.8)$$

where \dot{m}_p is the mass flow rate of the dispersed phase (kg/s) and Δt is the time step (s).

To carry out the simulation in HCCCT, not only the water spray distribution system but the simplification of the operation at the internal and external part of the cooling tower is required as well.

The spray water is injected into the tower through nozzles from the top of the tower and the distribution of the water was such that the horizontal component of the droplet velocity for each nozzle varied in such a way that the spray water could cover the whole width of the coil bank. The mean diameter of the water droplet is estimated from the terminal velocity of the droplets at a mean velocity of air flowing over the coil bank.. The air velocity at the inlet remains constant at 3.1 m/s. It has been observed that the temperature of the coils increases a bit with the increase of the iteration due to the assumption of the volumetric heat generation at the heat exchanger. To overcome this difficulty, Gan et al. [10] suggested that a linear heat flux should be distributed over the heat exchanger based on the assumption that, for same overall sensible heat transfer, the heat transfer rate varies in such a way that the transfer rate at the top row is twice that at the bottom row.

Boundary conditions

When a water droplet reaches into a boundary cell, the following boundary conditions are used at the tube coil, water droplets reflect as well as changes in its normal and tangential velocities. The coils are modeled as conducting walls with volumetric heat generation. Water droplets are assumed to reflect perfectly at the sidewalls of the HCCCT as well as on the symmetry plane. It is further assumed that when droplets fall down to the water basin at the

bottom, those escape and that the sticking droplet to the top wall is carried over by the air forced by fan.

The temperature range of the cooling water w.r.t. wet bulb temperature

The variation of the temperature range of the cooling water with respect to wet bulb temperature having a variable cooling water flow rate is shown in Fig. 3.7. The heat exchanger's common feature/trend that the temperature range decreases with both the increases of the WBT and the cooling water flow rate and vice versa as can be seen from this figure as well. In the standard condition, the temperature range found is around 4°C at WBT 27°C.

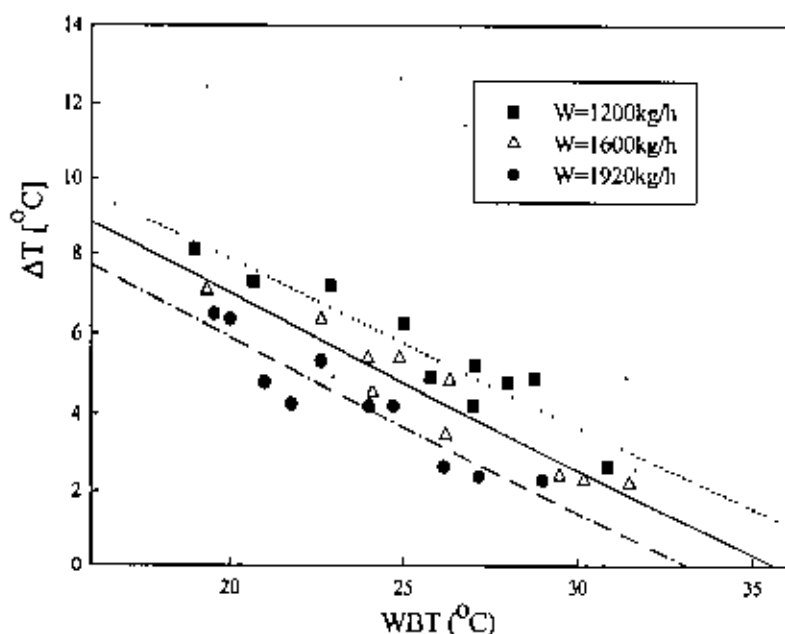


Fig 3.7 The temperature range of the cooling water w.t.to WBT

The cooling capacity in wet mode operation w.r.t. WBT

The cooling capacity in wet mode operation of the HCCCT w.r.t. WBT having different cooling water flow rate has been shown in Fig 3.8. It can be seen that the cooling capacity increases with the increase of the cooling water flow rate but decreases with the increase of the WBT followed by the decrease of the cooling water flow rate. At the design condition, the capacity at a WBT of 27°C was about 6400 kcal/h, which is 18% lower than the rated one. The assumed cooling water mass flow rate of 1600 kg/h could be a reason.

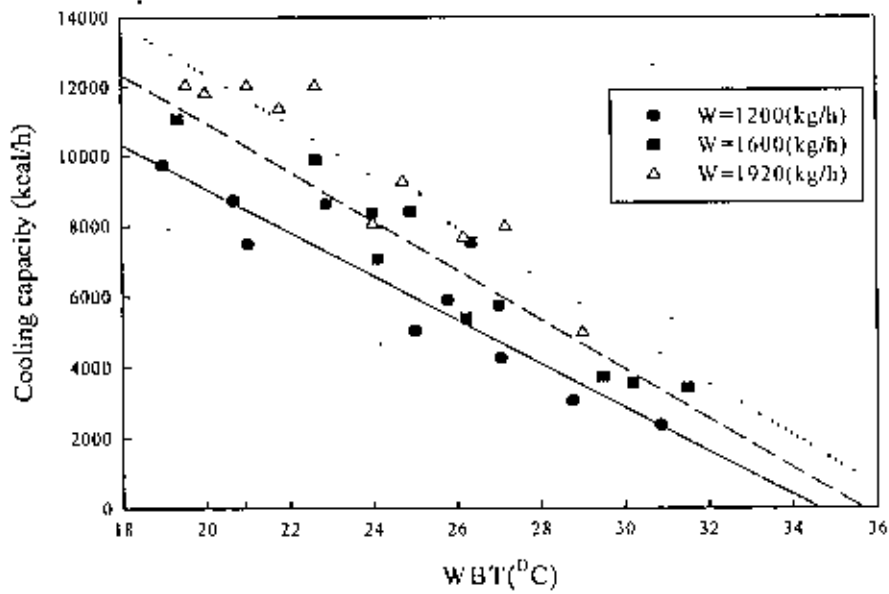


Fig. 3.8 The cooling capacity in wet mode operation w.r.t. WBT

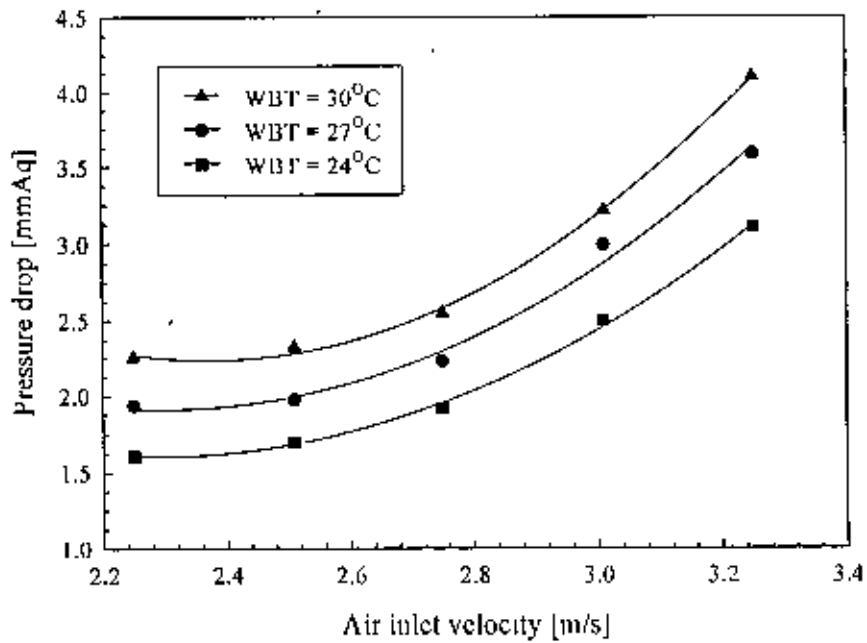


Fig.3.9 The pressure drop inside 2RT HCCCT in wet mode

The pressure drop with variable airflow rate

The pressure drop inside the heat exchanger of the HCCCT with respect to WBT having variable airflow rate has been shown in Fig. 3.9. Pressure drop is seen to increase with the increase of both the airflow rate and the WBT. For the standard condition, that is, at an airflow of 2.75 m/s and at WBT = 27°C, static pressure drop was to be 2.2 mmAq and the about 3.3 mmAq for the air velocity of 3.1 m/s.

3.4 Conclusion

Numerical simulation has been performed for the HCCCT having rated capacity of 2 RT. The temperature distribution is seen to decrease almost linearly for the increase of the air velocity and for the highest air velocity of 3 m/s, the temperature drop is the highest which is about 1.48°C and at a simulation condition of 2.75 m/s, the temperature drop is 1.37°C. Therefore, the cooling capacity of the 2 RT HCCCT is about 2192 kcal/h. At the simulation condition of 37°C, the temperature drop with respect to cooling water inlet temperature is 1.35°C. Therefore, the cooling capacity is about 2160 kcal/h. At the simulation condition of 15°C, the temperature drop with respect to air inlet temperature is 1.37°C. The cooling capacity is about 2192 kcal/h. The air inlet at the side wall coil having a transverse pitch of 45 mm produced lower pressure drop which was about 2.05 mmAq. In the standard condition, the temperature range of the cooling water found is around 4°C at WBT 27°C. At the design condition, the cooling capacity in wet mode operation at a WBT of 27°C was about 6400 kcal/h, which is 18% lower than the expected one. The assumed cooling water mass flow rate of 1600 kg/h could be a reason. For the standard condition, that is, at an airflow of 2.75 m/s and at WBT = 27°C, static pressure drop was to be 2.2 mmAq and the about 3.3 mmAq for the air velocity of 3.1 m/s.

Chapter Four

Conclusion

In this final chapter, the summary of the whole study has been discussed followed by a roadmap for extending the work further.

4.1 Summary of the thesis

In this thesis, the numerical study on the hybrid closed circuit cooling tower having a rated capacity of 2RT has been done. In this investigation, flow characteristics have been analyzed using the generalized non-orthogonal coordinate system. The internal flow fields have been numerically studied by solving the laminar type viscous model and problems related to pressure-velocity coupling were handled using the SIMPLE algorithm. The governing equations were discretized by means of control volume method and the discretized equations were solved by the tri-diagonal matrix algorithm.

In chapter 1, concept and the background of the hybrid closed circuit cooling tower were discussed.

In chapter 2, the basic equations in conservative form have been derived using generalized non-orthogonal coordinate system. The codes were verified with the published results and found to produce satisfactory results when applied to the lid driven cavity flow.

In chapter 3, numerical simulation has been performed for the HCCCT. In dry mode, at a simulation condition, that is at an air velocity of 2.75 m/s, the temperature drop was 1.37°C. Therefore, the cooling capacity of the HCCCT was about 2192 kcal/h. The temperature drop with respect to cooling water inlet temperature was 1.35°C and hence the cooling capacity was about 2160 kcal/h. The temperature drop with respect to air inlet temperature was 1.37°C and the capacity was about 2192 kcal/h.

In wet mode operation, the temperature range of the cooling water found was around 4°C at WBT 27°C and hence at the nominal simulating condition, the cooling capacity was about 6400 kcal/h, which is 18% lower than the rated one.

When the air inlet was located at the side wall of the HCCCT and having a transverse pitch of 45 mm produced lowest pressure drop in both modes. In dry mode, the pressure drop at an air velocity of 3.1 m/s was about 2.05 mmAq and in wet mode, the pressure drop was 2.2 mmAq and 3.3 mmAq for the air velocity of 2.75 m/s and 3.1 m/s respectively.

The results obtained from the numerical study of the performance characteristics of HCCCT is expected to serve as basic data that could be referred for the optimum design of the hybrid type closed circuit cooling tower.

4.2 Future work

Here are some ideas to form the basis of future work:

Two dimensional flow field as well as temperature distribution have been studied in this work. Future study can be extended to include the related phenomenon for three dimensional cases. The design parameters can be adjusted/changed to analyze the thermal performance of HCCCT having a rated capacity as high as 60 RT which can be applied in moderate sized establishments. Change of working fluid could open another gateway to the new horizon. Compressible flow can also be explored in future works.

References

- [1] Bergstrom, D.J; Derksen, D; Rezkallah, K.S; Numerical study of wind flow over a cooling tower, *Journal of wind engineering and industrial aerodynamics*, Vol. 46, No. 47 (1993), pp.657-664.
- [2] Bender, T.J; Bergstrom, D.J; Rezkallah, K.S; A study on the effects of wind on the air intake flow rate of a cooling tower; Part 3. Numerical study, *Journal of wind engineering and industrial aerodynamics*, Vol. 64, No.1 (1996), pp.73-88.
- [3] Bormoff, R.B; Mokhtarzadeh-Dehghan, M.R; A numerical study of interacting buoyant cooling-tower plumes, *Atmospheric environment*, Vol.35, No.3 (2001), pp.589-598.
- [4] Majumdar, A.K; Singhal, A.K; and Spalding, D.B; Numerical modeling of wet cooling towers. Part I, Mathematical and physical models. *ASME J. Heat Transfer*, Vol. 105, No. 4 (1983), pp. 728-735.
- [5] Hawlader, M. N. A; Liu, B. M; Numerical study of the thermal-hydraulic performance of evaporative natural draft cooling towers, *Applied Thermal Engineering*, Vol. 22, No. 1, (2002), pp. 41-59.
- [6] Dreyer, A. A; Erens, P. J; Modeling of cooling tower splash pack, *International Journal of Heat and Mass Transfer*, Vol. 39, No. 1, (1996), pp. 109 -123.
- [7] Jameel-Ur-Rehman Khan, Yaqub, M; Syed, M. Z; Performance characteristics of counter flow wet cooling towers, *Energy Conversion and Management*, Vol. 44, No. 13, (2003), pp. 2073-2091.
- [8] Ala Hasan, Guohui Gan, Simplification of analytical models and incorporation with CFD for the performance predication of closed-wet cooling towers, *International journal of energy research* Vol. 26, No. 16 (2002), pp.1161-1174.

- [9] Jaber, H; and Webb, R.L; Design of cooling towers by the effectiveness-NTU method. *ASME J. Heat Transfer*, Vol. 111, No. 4 (1989), pp. 837-843.
- [10] Gan, G; Riflat, S.B; Shao, L; Doherty, P; Application of CFD to closed-wet cooling towers, *Applied Thermal Engineering*, Vol., 21, No. 1 (2001), pp. 79-92.
- [11] Eldessouky, H. T. A; Alhaddad, A; Aljuwayhel, F. A; Modified analysis of counter flow wet cooling towers, *ASME Journal of Heat Transfer*, Vol. 119, No. 3 (1997), pp. 617-626.
- [12] Soylemez, M. S; On the optimum performance of forced draft counter flow cooling towers, *Energy Conversion and Management*, Vol. 45, No. 15-16 (2004), pp. 2335-2341.
- [13] Kloppers, J.C; Kroger, D.G; A critical investigation into the heat and mass transfer analysis of counterflow wet-cooling towers, *International Journal of Heat and Mass Transfer*, Vol. 48, No. 3-4 (2005), pp. 765-777.
- [14] Kaiser, A.S; Lucas, M; Viedma, A; and Zamora, B; Numerical model of evaporative cooling processes in a new type of cooling tower, *International Journal of Heat and Mass Transfer*, Vol. 48, No. 5 (2005), pp. 986-999.
- [15] Kunxiong Tan and Shiming Deng, A numerical analysis of heat and mass transfer inside a reversibly used water cooling tower, *Building and environment*, Vol. 38, No. 1 (2003), pp. 91-97.
- [16] Ibrahim, G.A; Nabhan, M.B.W; Anabtawi, M.Z; An investigation into a falling film type-cooling tower. *Int. J. Refrig*, Vol. 18 (1995), pp. 557-564.
- [17] Baker, D. R; and Shryock, H. A; A comprehensive approach to the analysis of cooling tower performance, *J. of Heat Transfer*, Vol. 83, No. 3 (1961), pp. 339-350.

- [18] Webb, R. L; A unified theoretical treatment for thermal analysis of cooling towers, evaporative condensers, and fluid coolers, ASHRAE Trans., Vol. 90, No. 2 (1984), pp. 398-415.
- [19] Webb, R. L; Villacres, A; Algorithms for performance simulation of cooling towers, evaporative condensers, and fluid coolers, ASHRAE Trans., Vol. 90, No. 2 (1984), pp. 416-458.
- [20] Al-Nimr, M. A; Dynamic thermal behavior of cooling tower, Energy conversion and management, Vol. 39, No. 7 (1998), pp. 631-636.
- [21] Makkinejad, N; Temperature profile in countercurrent/cocurrent spray towers, International Journal of Heat and Mass Transfer, Vol. 44, No. 2 (2001), pp. 429-442.
- [22] Pascal Stabat, Dominique Marchio, Simplified model for indirect-contact evaporative cooling-tower behavior, Applied Energy, Vol. 78, No. 4 (2004), pp. 433-451.
- [23] Suhas V. Patankar, Numerical heat transfer and fluid flow, Hemisphere Pub. Corp., McGraw-Hill, 1980.
- [24] John, D; Anderson, Jr; Computational fluid dynamics: the basics with applications, McGraw-Hill, New York, 1994.
- [25] Botella, R; Peyret, Benchmark spectral results on the lid-driven cavity flow, Computers & Fluids, Vol. 27, No. 4 (1998), pp. 421-433.
- [26] Sarker, M. M. A; Kim, E. P; Moon, C. G; Yoon, J. I; Thermal performance characteristics of closed-wet cooling tower, J. of the Korean Society for Power System Engineering, Vol. 9, No. 2 (2005), pp. 88-92.

